Development/Plasticity/Repair

STK25 and MST3 Have Overlapping Roles to Regulate Rho GTPases during Cortical Development

Tohru Matsuki,[1] Akio Iio,[1,2] Masashi Ueda,[1] Yumi Tsuneura,[1] Brian W. Howell,[3] and Atsuo Nakayama[1,4]
[1]Department of Cellular Pathology, Institute for Developmental Research, Aichi Developmental Disability Center, Kasugai 480-0392, Japan, [2]Biogate Co. Ltd., Gifu 501-2123, Japan, [3]Department of Neuroscience and Physiology, SUNY Upstate Medical University, Syracuse, New York 13210, and [4]Laboratory of Neurochemistry, Nagoya University Graduate School of Medicine, Nagoya 466-8560, Japan

Precise control of neuronal migration is required for the laminar organization of the neocortex and critical for brain function. We previously reported that the acute disruption of the *Stk25* gene (*Stk25* conditional knock-out; cKO) during mouse embryogenesis causes anomalous neuronal migration in the neocortex, but paradoxically the *Stk25* cKO did not have a cortical phenotype, suggesting some forms of compensation exist. In this study, we report that MST3, another member of the GCKIII subgroup of the Ste20-like kinase family, compensates for loss of *Stk25* and vice versa with sex independent manner. MST3 overexpression rescued neuronal migration deficit and abnormal axonogenesis in *Stk25* cKO brains. Mechanistically, STK25 leads to Rac1 activation and reduced RhoA levels in the developing brain, both of which are required to fully restore neuronal migration in the *Stk25* cKO brain. Abnormal migration phenotypes are also rescued by overexpression of Bacurd1and Cul3, which target RhoA for degradation, and activate Rac1. This study reveals that MST3 upregulation is capable of rescuing acute *Stk25* deficiency and resolves details of signaling downstream STK25 required for corticogenesis both common to and distinct from MST3 signaling.

Key words: **genetic compensation; MST3; neuronal migration; neuronal polarization; Rho GTPases regulation; STK25**

Significance Statement

Proper neuronal migration during cortical development is required for normal neuronal function. Here, we show that STK25 and MST3 kinases regulate neuronal migration and polarization in a mutually compensatory manner. Furthermore, STK25 balances Rac1 activity and RhoA level through forming complexes with α-PIX and β-PIX, GTPase regulatory enzymes, and Cullin3-Bacurd1/Kctd13, a pair of RhoA ubiquitination molecules in a kinase activity-independent manner. Our findings demonstrate the importance of overlapping and unique roles of STK25 and MST3 to regulate Rho GTPase activities in cortical development.

Introduction

Abnormal cortical development caused by defects in neuronal migration often led to intellectual disability, epilepsy, and autism spectrum disorder. As the many classes of neurons that co-localize in the mature brain are produced in distant germinal zones at distinctive developmental stages, neuronal migration needs to be carefully choreographed. This is best understood in the neocortex where a multitude of genetic pathways are known to play a role in its laminar organization (Barnes and Polleux, 2009; Cooper, 2014). The excitatory neurons that are produced at distinct times in the underlying ventricular zone (VZ) and ultimately migrate to distinct layers of the mature cortex, correspond to different neuronal identities. Many of the gene products that regulate positioning have important roles in the signaling systems that regulate the motile forces generated by cytoskeletal dynamics.

The STK25 kinase is involved in the regulation of neuronal migration, in addition to cell polarization, Golgi apparatus morphology, glucose and lipid metabolism, and Hippo signaling (Preisinger et al., 2004; Matsuki et al., 2010; Amrutkar et al.,

Received Mar. 10, 2021; revised Aug. 13, 2021; accepted Sep. 6, 2021.

Author contributions: T.M. designed research; T.M., A.I., and Y.T. performed research; T.M., M.U., B.W.H., and A.N. contributed unpublished reagents/analytic tools; T.M. and A.I. analyzed data; T.M. wrote the first draft of the paper; T.M., A.I., B.W.H., and A.N. edited the paper; T.M. and B.W.H. wrote the paper.

This work was supported by funds from the research grant of The Japan Foundation for Pediatric Research (T.M.); the Naito Foundation (T.M.); Takeda Science Foundation (T.M.); and Japan Society for the Promotion of Science (JSPS) Grants-in-Aid for Scientific Research (KAKENHI) 25890026 (to T.M.), 15K06795 (to T.M.), 24591693 (to A.N.), and 26460483 (to A.I.). We thank Akie Toya for experimental assistance; Hans Clevers (Hubrecht Institute) for cell lines; Shuji Miyagawa (Osaka University), Hideki Murakami (Aichi Medical University), Hidenori Ito, Hidenori Tabata, Koh-ichi Nagata (Institute for Developmental Research), and Jun-ichi Miyazaki (Osaka University) for DNA vectors; Ikuyo Mizuguchi and Eri Yorifuji (division for medical research engineering, Nagoya University Graduate School of Medicine) for assistance with confocal microscopy; and Masato Asai and Machiko Iida (Institute for Developmental Research) for assistance with histological staining.

M. Ueda's present address: Department of Mental Retardation and Birth Defect Research, National Center of Neurology and Psychiatry, Tokyo 187-8502, Japan.

The authors declare no competing financial interests.

Correspondence should be addressed to Tohru Matsuki at matsukit@inst-hsc.jp.

https://doi.org/10.1523/JNEUROSCI.0523-21.2021

2016; Lim et al., 2019; Bae et al., 2020). We previously demonstrated that acute *Stk25* knock-out (KO) impedes neuronal migration (Matsuki et al., 2013). However, constitutive *Stk25*-null mutant mice do not have similarly disrupted neuronal migration (Matsuki et al., 2013); therefore, an unknown molecule may compensate for *Stk25*'s absence in these mice. In other situations where the KO of a gene has no observed phenotype but the knock-down does, increased expression of a related gene has on occasion been shown to be responsible for the genetic compensation (El-Brolosy and Stainier, 2017). Since the genetic response to the deficit is not instantaneous, if the genetic deficiency is induced during a critical time frame it leads to a phenotype, while if the deficiency is present from inception genetic compensation is capable of functional rescue.

Recent reports indicate that MST3, a member of the GCKIII subfamily like STK25, is also involved in neuronal migration and axon formation (Lorber et al., 2009; Tang et al., 2014) . MST3 also has roles in axon regeneration. Its re-expression in *Mst3* knock-down dorsal root ganglion neurons induces axon regeneration *in vivo* (Lorber et al., 2009). MST3 and STK25 share 71.8% protein sequence identity, suggesting that MST3 and STK25 may have similar regulation and substrates. One key MST3 substrate involved in neuronal migration is RhoA, which MST3 reportedly phosphorylates and inactivates (Tang et al., 2014); however, STK25 is not known to phosphorylate RhoA.

The Rho GTPases regulate neuronal migration in addition to the migration of several other cell types, including tumor cells (Kholmanskikh et al., 2003; Kawauchi, 2011; Lawson and Ridley, 2018). Rho GTPases' roles extend to many other cellular functions as well (Lawson and Ridley, 2018). Such broad function are also apparent in neuronal development, making it difficult at times to dissociate their roles in neuronal differentiation from those in migration (Govek et al., 2011). However, by carefully inactivating the Rho GTPases in postmitotic neurons, it has become clear that they have distinct roles in neuronal migration. Rac1 deficiency, for instance, leads to a reduction in the speed of radial migration of cortical neurons, which results in a larger percentage of neurons found outside of the cortical plate during neocortical development (Chen et al., 2007). CDC42 has a similar positive role to promote neuronal migration as part of a complex with Lis1, IQGAP1 and CLIP-170 (Kholmanskikh et al., 2006). On the other hand, RhoA appears to suppress neuronal migration. Its levels are highest in premigratory cells (Olenik et al., 1999) and ectopic expression of RhoA blocks radial migration, whereas suppressing RhoA promotes migration (Kholmanskikh et al., 2003; Pacary et al., 2011).

In this study, we demonstrate that STK25 activates Rac1 as well as targets RhoA for degradation, both of which are required for normalization of radial migration in *Stk25* conditional KO (cKO) brains. STK25 kinase function is not required for this since the kinase-inactive STK25, in which K49R substitution was introduced, is capable of rescuing the defect. Instead STK25 appears to act as a scaffolding molecule forming protein-protein interactions with key regulators of the Rho GTPases. Furthermore, our study shows that MST3 levels increase in response to *Stk25* deficiency with a delayed of 3–4 d and that exogenous MST3 rescues cell polarization, axonogenesis, and migration in neurons lacking *Stk25*.

Materials and Methods

Mice

All animals were used in accordance with the protocol approved by the Animal Committee of the Institute for Developmental Research. Timed-pregnant C57BL/6J wild-type (WT) female mice were purchased from Japan SLC. *Stk25*$^{fl/fl}$ (Matsuki et al., 2013) and *CAGGCre-ER*^{TM} (stock #004682, The Jackson Laboratory) mice have been described before and were maintained on the C57BL/6J strain. Both male and female embryos were used for immunohistochemistry, *in vitro* experiments, and *in utero* electroporation.

Mouse hippocampal neuron culture

Hippocampal neurons were isolated from embryonic day (E)16.5 mice and grown in Neurobasal medium supplemented with 2% B27 and Glutamax-I (Thermo Fisher Scientific). For polarity studies, the neurons ($2–3 \times 10^4$ cells/cm^2) were infected with the respective viruses on the day of culturing and were replaced 2 d later on poly-L-lysine coated coverslips. Axons were defined as SMI-312-positive processes >80 μm after 2 d of culture.

Cell culture

Human embryonic kidney (HEK)293FT cells and W4 intestinal epithelial cells were cultured with DMEM containing 10% FBS and penicillin/streptomycin. All cell lines were confirmed to be mycoplasma free using a mycoplasma detection kit (MycoAlert, Lonza) and cultured with 5% CO_2 at 37°C.

Expression vectors

The pLLC vector contains double promoters that expresses shRNA (driven by the U6 promoter) and marker GFP (driven by a CAG promoter; Matsuki et al., 2010). The pLS vectors, used for overexpression, have the human Synapsin I (hSYN) promoter driving neuron specific expression. Both lentiviral vectors were modified versions of pLL3.7 (Addgene #11795). RFP alone, MST3 WT-RFP, and MST3-K53R-RFP were expressed under the hSYN promoter. The shRNA constructs to knock-down mouse and human *STK25* and *LKB1* expression were the same as described in our previous study (Matsuki et al., 2010), and the shRNA sequences to knock-down *Mst3* were based on the Sigma MISSION shRNA Library of the RNAi Consortium; TRCN0000025241 (#1) GCCTGGCCCTTTAGATGAAAT, TRCN0000025242 (#2) CTCT CAGTGTTTATCCACAAT, TRCN0000276662 (#3) TCCCTTGGC ATCACCGCAATA. The shRNA sequences to knock-down human *MST3* were based on the Sigma MISSION shRNA Library of the RNAi Consortium; TRCN0000199367 (#1) CCCTGGGCATAACAGCTA TTG, TRCN0000000645 (#2) TGCAGAGTTGAAGGAGAAGAG, TRCN0000195637 (#3) CCCACTGCTAAGGAGTTATTG. The shRNA sequences to knock-down *RhoA* were based on the Sigma MISSION shRNA Library of the RNAi Consortium; TRCN0000304690 (#1) ACGCAGCCTCATGCGGTTAAT, TRCN0000304743 (#2) ATTGACA GCCCTGATAGTTTA, TRCN0000302388 (#3) GTCAAGCATTTCTG TCCAAAT. We used the same STK25 expression vectors as in our previous report (Matsuki et al., 2010). The MST3 K53R expression vector was generated by PCR-based mutagenesis in accordance with a previous study (Tang et al., 2014). FLAG epitope tag fused RhoA, all Rac1 (WT, V12 and N17 mutant), and Cdc42 were amplified and cloned into pCAGGS vectors (Niwa et al., 1991). pcDNA3-myc-Cul1, Cul2, Cul3, Cul4A, Cul4B, Cul5, and Cul7 were purchased from Addgene. The FANTOM clones of mouse Bacurd1 (clone ID 1500003N18) and 2 (clone ID 1200004D17) were purchased from DNAform. The myc epitope tags were fused to Bacurds by PCR and inserted into the pCAGGS vector. pCNX-Cre was used for the acute deletion of the *Stk25* gene.

Antibodies

We used the following antibodies for immunoblotting, immunoprecipitation (IP), immunocytochemistry, and immunohistochemistry: anti-STK25 (Matsuki et al., 2010), anti-RhoA, anti-MST3, and anti-MST4 (ab51137, ab187027, ab52491, Abcam), anti-β-Actin (AC-15, Sigma), anti-CYFIP1/Sra-1 (07-531, Millipore), anti-myc tag conjugated with HRP (014-21901, Wako Chemical), anti-DYKDDDDK (FLAG) tag conjugated with HRP (018-22381, Wako Chemical), anti-GST conjugated with HRP (011-21891, Wako Chemical), anti-HA conjugated with HRP (12013819001, Roche), anti-DYKDDDDK (FLAG)-tag (14793, Cell Signaling), anti-Rac1 (610650, BD Transduction Lab), anti-GFP

(A10262, Thermo Fisher Scientific), anti-pan-axonal neurofilament marker SMI-312 (SMI-312R, Covance; used for Fig. 3*A–F*,*H–M*; data not shown), and anti-RFP (600-401-379, Rockland), anti-Cul3, anti-Cul4, anti-Bacurd1, and anti-Bacurd2 (sc-166110; used for Fig. 10*B*,*G*, sc-377188; used for Fig. 10*C*,*H*, sc-393994; used for Fig. 10*D*, *I*, and sc-515765; used for Fig. 10*E*,*J*, Santa Cruz) antibodies.

IP and immunoblotting

HEK293FT cells (1×10^5 cells/cm^2 in a six-well cell culture dish) were cultured 1 d before transfection, which was performed using X-tremeGENE HP (Roche) in accordance with the manufacturer's instructions. Briefly, 2 µg of each pCAGGS vector (Niwa et al., 1991) were mixed with 2 µl of transfection reagent and applied to the cells after 15-min incubation. The cells were cultured for 48 h after transfection before harvesting. They were then lysed with NP40 cell lysis buffer (NP40-IPB; 137 mM NaCl, 2.7 mM KCl, 1% IGEPAL CA-630, 25 mM Tris-HCl, pH 7.4, 2 mM EDTA, 50 mM NaF, 0.1% 2-mercaptoethanol, protease inhibitor cocktail; cOmplete Mini, EDTA-free; Roche), 1 mM sodium orthovanadate, and 1 mM phenylarsine oxide) and clarified by centrifugation at $20{,}000 \times g$ for 10 min. The clarified cell lysates for IP were incubated with magnetic beads linked to Protein G (SureBeads, Bio-Rad) and antibody for 30 min at 4°C. Immunocomplexes were separated from the lysis buffer by magnetic separation and washed 3× with ice-cold NP40-IPB. The elution was performed using 1× sample buffer (62.5 mM Tris-HCl, pH 6.8, 25 mM dithiothreitol, 2% SDS, 10% sucrose, and 0.004% bromophenol blue) and resolved by SDS-polyacrylamide gel (10% or 14%) electrophoresis. The resolved samples were transferred to a PVDF membrane (Immobilon-P, Millipore) and subjected to immunoblotting with the appropriate antibodies in 0.1% Tween, 150 mM NaCl, and 20 mM Tris-HCl, pH 7.4, containing buffer (TTBS). All immunoblot images were captured with a LAS 4000 camera system (General Electric).

Immunostaining for agarose-embedded sections and cultured cells

Immunocytochemistry was conducted according to our previous study (Matsuki et al., 2010). Cultured mouse hippocampal neurons and W4 cells were fixed with 4% paraformaldehyde (PFA), 250 mM sucrose, 2.5 mM KCl, 2.5 mM magnesium acetate, and 25 mM HEPES, pH7.4 (PFA fixation buffer) for 10 min at 25°C. Fixed cells were treated with 0.1% saponin in PBS for 10 min at 25°C for permeabilization. The cells were further processed with 3% BSA and incubated with 10% normal goat serum, including 0.05% sodium azide in TTBS for at least 30 min at 25°C. To stain for F-actin, phalloidin conjugated with fluorescent dye was diluted with 0.1% BSA in PBS and incubated for 30 min at 25°C. For immunohistochemistry, 50-µm thickness brain sections were prepared using a vibratome (Leica VT1000 S) after perfusion with 4% PFA solution and embedding in 3% agarose in PBS. Each section was incubated with 5% BSA containing blocking buffer (BB; containing 0.25% Triton X-100 in place of Tween 20) for 1 h at 25°C and incubated with the primary antibody overnight at 4°C. The sections were washed with the BB 3× and incubated with secondary antibodies in BB for 2 h at 25°C. All images were taken using a Zeiss LSM 880 confocal microscopy system.

Cell polarity assay using W4 cells

W4 cells were infected with indicated viruses to knock-down *Stk25* or *Mst3* 1 d before transfection. The myc-tagged STK25 WT, STK25 K49R, MST3 WT, or K53R expressing plasmids were transfected using X-tremeGENE HP (Roche) on the next day. Cells were exposed to 2 microM doxycycline (Dox) containing culture medium for 24 h from 1 d after transfection. Cells were fixed with 4% PFA fixation buffer for 10 min at room temperature. Cell were permeabilized with 0.1% saponin containing PBS for 10 min at room temperature and subsequently immunostained with indicated antibodies. Filamentous actin was visualized using phalloidin conjugated with CF 568 (Biotium).

Immunohistochemical staining for paraffin-embedded sections

E15.5 mouse embryos were isolated and perfused with 4% PFA fixation buffer (4% PFA, 250 mM sucrose, 2.5 mM KCl, 2.5 mM Mg $(CH_3COO)_2{\cdot}4H_2O$, 25 mM HEPES; pH 7.4). The perfused embryos were then postfixed in PFA solution for 1 h. The fixed embryos were immersed in 70% EtOH for at least 2 d. To clarify the precise expression of endogenous STK25, MST3, and MST4 in E15.5 mouse embryo, we used low melt paraffin (Paraplast X-TRA, P3808, Sigma; Fig. 1*Be–l*). The paraffin exchange process was performed using the following steps for 2 h each: 70% EtOH, 80% EtOH, 90% EtOH, 3× 100% EtOH, 3× xylene, and 3× paraffin steps. Each embryo was embedded in paraffin and processed for sectioning at thickness of 4 or 6 µm. The sections were then stained using each antibody and Agilent EnVision+ or with hematoxylin-eosin (Fig. 1*Ba*,*e*,*i*, 8*Aa*,*c*,*e*, *g*, 10*A*,*F*). All images were taken using an Olympus MVX10 camera and a Nikon E800 microscope.

Quantitative PCR analysis

Total RNA was extracted from the cultured cells and half of the hemisphere from *Stk25*$^{fl/fl}$ with/without Cre-ER mice at E16.5 and E18.5 using an RNA isolation kit (NucleoSpin RNA Plus, Macherey-Nagel). The qPCR template was prepared using ReverTra Ace qPCR RT Master Mix (Toyobo). RT-PCR analysis was conducted using THUNDERBIRD SYBR qPCR Mix (Toyobo) and a CFX96 Touch Real-Time PCR Detection System (Bio-Rad), with the following primer sets: for mouse *Stk25*, CGCAAGATCCACCGAGATA and CTGCCAGCTTCACA TCACC; for mouse *Mst3*, GCAGTCAGCCTACGACTCAA and GCC AGTTCTATTGCGGTGAT; for mouse *β-Actin*, CTAAGGCCAACC GTGAAAAG and ACCAGAGGCATACAGGGACA. *Stk25* and *Mst3* expression data were normalized to *β-Actin* levels and averaged across three separate experiments conducted in triplicate with three independently generated RNA samples.

In utero *electroporation*

For *in utero* electroporations, DNA was mixed with Fast Green dye in PBS and injected into half of the lateral ventricle of E14.5 embryos. Electrostimulations were applied to the embryos at 40 V with 100-ms intervals 4× using NEPA21 super electroporator (NEPA gene). To examine neuronal migration, embryos electroporated with the indicated plasmids were perfused with 4% PFA fixation solution 3 d after electroporation. Fixed brains were embedded with 3% Agarose and sectioned at 50-µm-thick for confocal microscopy analysis.

Lentivirus production

Lentiviral production was conducted in accordance with our previous report (Matsuki et al., 2010), with minor modifications. We used psPAX2 and pCMV-VSV-G-RSV-Rev as packaging vectors (Addgene, #12260 and gifted from Miyoshi). HEK293FT cells were grown to 90–95% confluency at the time of transfection. The transducing vector and packaging vectors were transfected using PEI max (25 kDa, Polyscience Inc.). The culture medium was replaced with fresh serum-reduced culture media (Opti-MEM I, ThermoFisher Scientific) that included penicillin/streptomycin 3 h after transfection. The virus-containing medium was collected 48 h after transfection and centrifuged to remove debris. Lentiviruses were concentrated using Amicon Ultra-15 (Millipore) before infecting cultured neurons.

Image analysis

Confocal images were collected with *z*-axis stacked optical sections ~30 µm thick. Each stacked image was projected to a 2D image for neuronal migration and neuron shape analysis using ZEN software (Zeiss). In addition, neurons subjected to the computer-based reconstruction analysis (Fig. 2*A*,*D*) were carefully selected by referring to 3D-rendered images. Image processing of the selected neuron shape was performed by thresholding (Adobe Photoshop) flattened 2D images. The axon and neurite lengths were analyzed with MetaMorph software (Molecular Devices; Figs. 2*B*,*C*,*E*,*F*, 3*G*,*O*, 4*B*).

Fluorescence resonance energy transfer (FRET) analysis

The Rac1 activation state FRET biosensor (pCAG-Raichu 1011×) was used to monitor Rac1-GTP levels and was kindly provided by Matsuda (Itoh et al., 2002; Kurokawa et al., 2004; Higashi et al., 2010). The Raichu plasmid with or without the Cre expressing plasmid was transfected into neuronal precursor cells at the ventricular surface at E14.5. We performed FRET analysis with fixed brain slices following previous reports

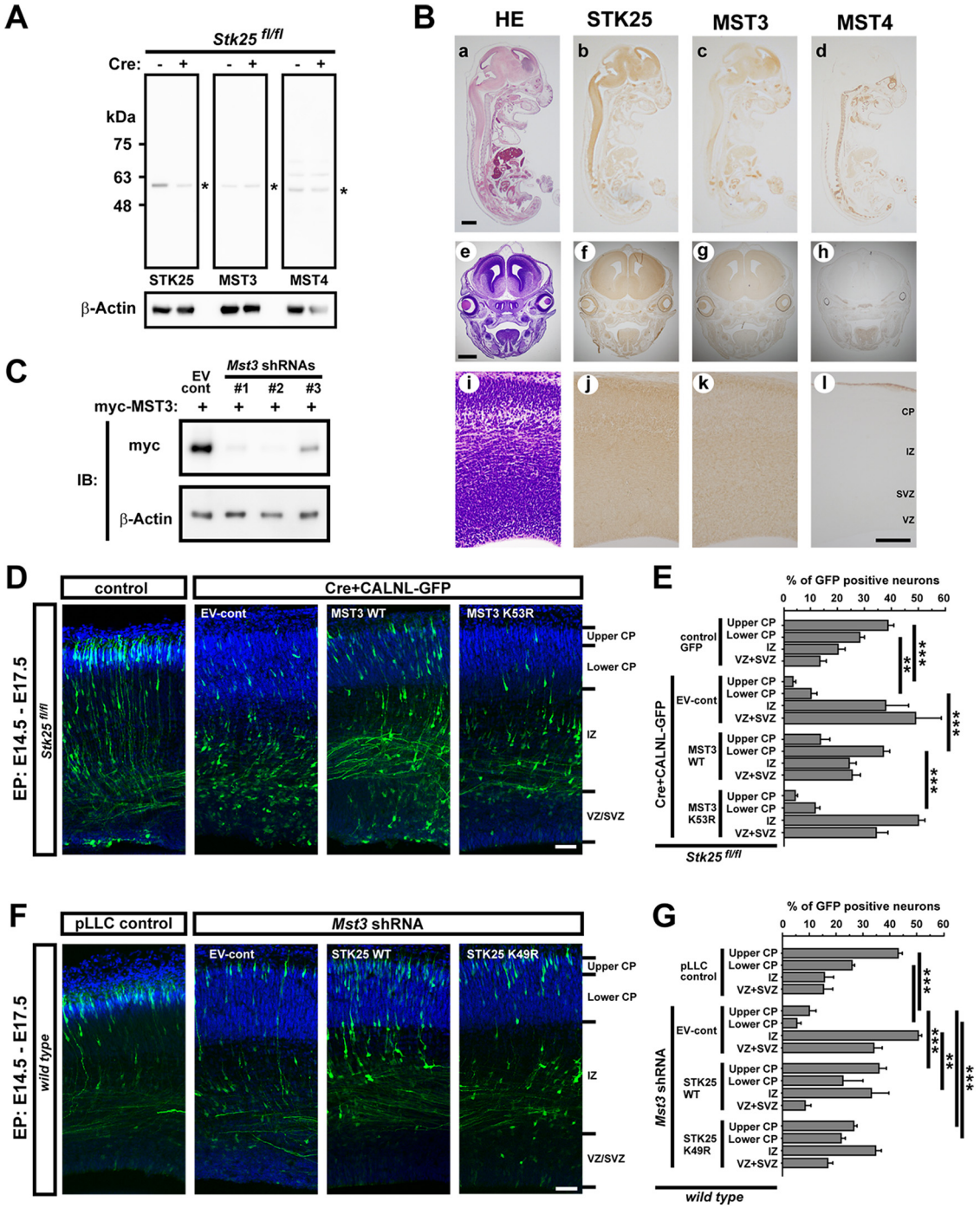

Figure 1. STK25 and MST3 have compensatory roles in neuronal migration. ***A***, We assessed specificity of anti-STK25, MST3, and MST4 antibodies by immunoblot. Each anybody was incubated with membrane including *Stk25*$^{fl/fl}$;+/+ and *Stk25*$^{fl/fl}$;*Cre-ER*^{TM} brain lysate. Both animals were exposed with tamoxifen at E14.5 and killed at E18.5. Upper panels show each immunoreactive signal. Lower panel shows β-Actin signals. Asterisks indicate each full-length molecule. ***B***, Immunohistochemical staining of paraffin-embedded sections of mouse embryos at E15.5. Upper panels are sagittal sections which show (***a***) hematoxylin-eosin (HE), (***b***) anti-STK25 antibody, (***c***) anti-MST3 antibody, and (***d***) anti-MST4 antibody staining, respectively. The order of the stains was maintained for the middle and lower panels that contain coronal sections (***e–h***) and magnified images of the cortex from the panels above (***i–l***). Scale bars: 1 mm (***a***, ***e***) and 50 μm (***l***). ***C***, We assessed the mouse *Mst3* shRNA knock-down efficiency from three candidates by co-expression with myc-MST3. The shRNAs, annotated as #1 and #2, showed similar knock-down effects. The shRNA #1 was used for all experiments in this study. ***D***, Co-electroporation of MST3 WT, but not MST3 K53R, a kinase-inactive version, partially rescued neuronal migration defects of *Stk25* cKO neurons electroporated at E17.5 following *in utero* electroporation at E14.5 (CP, cortical plate; IZ, intermediate zone; VZ/SVZ, ventricular zone and subventricular zone). Expression of Cre in *Stk25*$^{fl/fl}$ mice led to aberrant neuronal positioning (EV-cont panel). ***E***, Quantification of the population of GFP$^+$ neurons in the cortical layers of E17.5 *Stk25*$^{fl/fl}$ embryos as shown in ***D***. ***F***, Both WT STK25 and kinase-inactive STK25 (K49R) rescued neuronal migration defects caused by *Mst3* knock-down. ***G***, Quantification of the population of GFP$^+$ neurons in the cortical layers of E17.5 WT embryos as shown in ***F*** (**$p < 0.01$, ***$p < 0.001$, one-way ANOVA with Holm–Bonferroni *post hoc* test; error bars, SEM; scale bars: 50 μm).

(Pacary et al., 2011) with minor modification. We employed 2% PFA solution for perfusion and postfixation for 30 min and following sectioning (60 μm thick). All FRET images were obtained using a Zeiss LSM 880 confocal laser scanning microscope selected with Plan-Apochromat 63×/1.4 Oil objective lens following the previous report (Pacary et al., 2011). The CFP and YFP were excited using a 405-nm diode and 514-nm argon laser. Two emission channels were split using a spectral channel GaAsP detector; for CFP, the signal was in the 463- to 526-nm range,

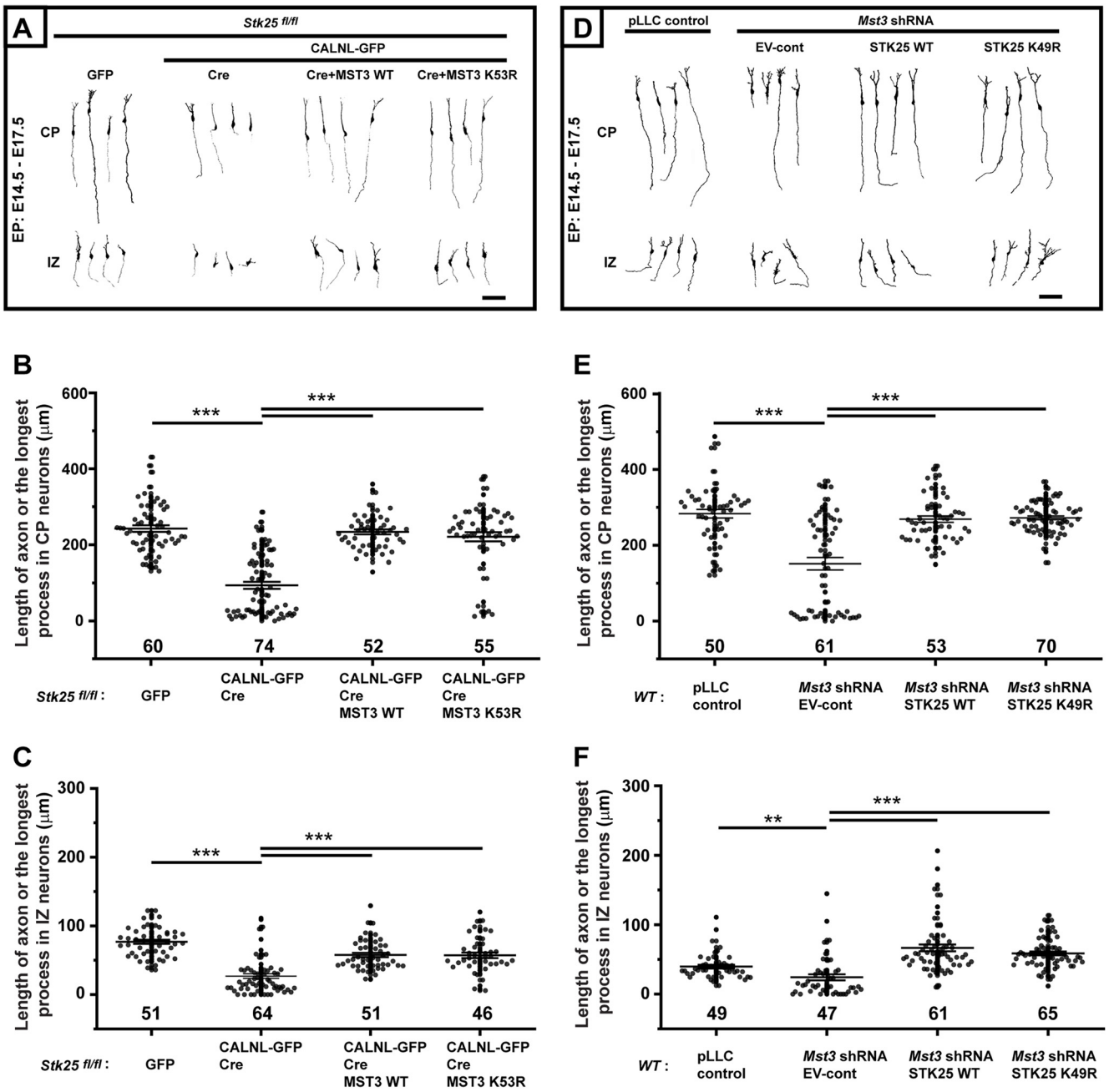

Figure 2. The axon formation in nascent neurons is rescued by overexpression of MST3 in acute *Stk25* KO and by STK25 in *Mst3* knock-down neurons. ***A***, ***D***, Computer-based reconstructed images of neurons at E17.5 after electroporations at E14.5. The upper images represent typical neurons from the cortical plate (CP), while the lower images represent typical neurons from the intermediate zone (IZ) of each genotype mouse transfected with indicated plasmids. The Cre-expressing plasmid induces abnormality in axonogenesis as compared with GFP alone. Both MST3 WT and MST3 K53R rescued axon generation in ***A***. *Mst3* shRNA results in absent or shorter-axon phenotypes in neurons as compared with vector alone controls. Overexpressing of STK25 WT and STK25 K49R rescued these phenotypes in ***D***. Scale bar: 50 μm. ***B***, ***C***, Quantitative analysis of the length of the axon or the longest process settled in cortical plate (***B***) or intermediate zone (***C***) shown in ***A***. The axonogenesis defect in *Stk25* cKO was statistically significant and recovered by MST3 overexpression with kinase activity independent manner. Each dot represents a single data spot from analyzed neuron. The number below each dataset shows the number of neurons analyzed from at least four brains. ***E***, ***F***, Quantitative analysis of the length of the axon or the longest process settled in cortical plate (***E***) or intermediate zone (***F***) shown in ***D***. The neuronal polarization defects in *Mst3* knock-down neurons showed statistically significant recovery with STK25 overexpression in a kinase activity-independent manner. The number below each dataset shows the number of neurons analyzed from at least three brains (**$p < 0.01$, ***$p < 0.001$, one-way ANOVA with Holm–Bonferroni *post hoc* test; error bars, SEM).

and for YFP, it was in the 535- to 633-nm range. Pinholes were opened and set at a 2 μm depth for each channel. Scanning was performed on a sequential, line-by-line basis for each channel with a 75% laser power. To analyze the FRET efficiency, the same setting for the acceptor photobleaching was applied to all samples. The time-lapse mode was set as five prebleaching imaging before postbleaching imaging. The photo-bleaching was performed at least 100 iterations with 514-nm laser with maximum power. The FRET ratio images were processed using ZEN software (Zeiss). FRET efficiency was calculated using the following formula: $FRET_{efficiency} = 1 - CFP_{prebleach}/CFP_{postbleach}$.

Statistical analysis

All experiments were performed in triplicate, at minimum. Comparisons among multiple groups with a control were analyzed using

one-way ANOVA with Holm–Bonferroni *post hoc* test. Comparisons between two groups with a control were analyzed using the Student's *t* test. All statistical analyses were performed using OriginPro 2020 (Origin Lab). Error bars indicate SEM.

Results

STK25 and MST3 regulate neuronal migration in a compensatory manner

The germline KO of *Stk25* does not cause apparent developmental deficiencies, whereas the acute disruption of *Stk25* at E14.5 leads to mispositioning of neurons during development (Matsuki et al., 2013). This suggests that an unknown molecule might compensate for the loss of *Stk25* during brain development. Since STK25, MST3, and MST4 belong to the same subfamily of Ste20-like kinases, MST3 and/or MST4 are likely candidates. MST3 and MST4 have 71.8% and 66.3% protein sequence homology with STK25, respectively. Accordingly, we first investigated their expression patterns in the mouse brain at E15.5 using antibodies that recognize each molecule (Fig. 1*A*,*B*). STK25 and MST3 immunostaining demonstrated pronounced expression in the brain, neuroretina and spinal cord (Fig. 1*Bb*,*c*,*f*,*g*,*j*,*k*). In contrast, the MST4 signal was absent from the brain, neuroretina and spinal cord but was expressed in the cartilage primordium at this stage (Fig. 1*Bd*,*h*,*l*). Focusing on the cerebral cortex, STK25 and MST3 immunoreactivity spanned all the layers of the developing brain, but MST4 was not detected (Fig. 1*Bj–l*). Thus, STK25 and MST3, but not MST4, could have similar biological functions during neuronal development. To determine whether MST3 function overlaps with that of STK25, we examined whether MST3 was able to rescue migration defects of neurons with a conditional disruption of *Stk25*. To study this, embryonic brains homozygous for the *Stk25* floxed allele ($Stk25^{fl/fl}$) were electroporated at E14.5 with expression vectors for GFP alone (control) or *CALNL-GFP*, a Cre recombination indicator (Matsuda and Cepko, 2007), with a combination of Cre and either empty vector (EV-control; EV-cont), MST3 WT or kinase-inactive form of MST3, in which K53R was introduced. The population of GFP-positive (GFP^+) neurons within each layer was analyzed at E17.5. *Stk25* gene inactivation by Cre expression resulted in significant losses of GFP^+ neurons from the upper and lower cortical plate ($p < 0.001$, upper; $p < 0.01$, lower; Fig. 1*D*,*E*). MST3's role in neuronal migration is kinase activity dependent since MST3 WT expression recovered migration to the cortical plate in *Stk25 cKO* neurons with exogenous ($p < 0.001$; Fig. 1*D*,*E*), whereas kinase-inactive form of MST3 overexpressing *Stk25*-deficient neurons were predominantly localized in the VZ and subventricular zone (SVZ), similar to *Stk25*-deficient neurons in the absence of MST3 expression (Cre + CALNL-GFP + EV-cont; Fig. 1*D*,*E*).

It has previously been reported that knock-down of *Mst3* causes a neuronal positioning defect similar to the one observed in *Stk25* knock-down and *Stk25* cKO neurons (Matsuki et al., 2013; Tang et al., 2014). Therefore, to determine whether STK25 can compensate for MST3 deficit, we knocked down *Mst3* in developing brain at E14.5 and simultaneously overexpressed STK25. Interestingly we found that both STK25 WT and kinase-inactive form of STK25 rescued impaired neuronal positioning in *Mst3* knock-down neurons in contrast with the EV-cont (Fig. 1*F*,*G*). This is in line with our previous findings that kinase-inactive form of STK25 can rescue the acute loss of *Stk25* function equally well as STK25 WT (Matsuki et al., 2013).

STK25 and MST3 regulate axonal formation *in vivo* in a compensatory manner

Axon formation is one of the first visible signs of neuronal polarization. We previously reported *Stk25* knock-down causes deficits in neuronal polarization and abnormal axonogenesis both *in vitro* and *in vivo* (Matsuki et al., 2010). In line with our previous observation, aberrant axonogenesis was observed in neurons at E17.5 after *Stk25* cKO at E14.5 (Fig. 2*A*). To determine whether MST3 and SKT25 act redundantly in axonogenesis *in vivo*, we investigated the effect of MST3 overexpression in these cKO mice. Both MST3 WT and kinase-inactive form of MST3 prevented the shortened axon phenotype caused by acute inactivation of *Stk25* in the brain (Fig. 2*A–C*). Furthermore, *Mst3* knock-down neurons also had shorter axons at E17.5 after electroporation of knock-down vectors at E14.5 *in vivo* (Fig. 2*D–F*). This was a similar phenotype to that of *Stk25* cKO neurons (Fig. 2*A–C*) and was similarly rescued by overexpression of both STK25 WT and kinase-inactive form of STK25 (Fig. 2*D–F*). Interestingly, the kinase activity of MST3 does not appear to be required for the regulation of neuronal polarization, whereas it is required to rescue neuronal migration defects in *Mst3*-deficient and *Stk25*-deficient neurons (Tang et al., 2014; Fig. 1*D*,*E*). Collectively, these results indicate that STK25 and MST3 have similar biological roles in axonal formation and neuronal migration *in vivo*, but these roles are not entirely complementary.

MST3 rescues abnormal cell-polarization phenotypes in *Stk25*-deficient cells in a compensatory manner

We further examined whether STK25 and MST3 had overlapping roles in neuronal polarization in cultured hippocampal neurons. The first polarizing event in neurogenesis is the formation of the axon and thus we quantified axon production. RFP or MST3-RFP fusion proteins were expressed in neurons infected with either the EV-cont or *Stk25* shRNA virus (Fig. 3*A–G*). Both MST3 WT and kinase-inactive form rescued axonogenesis in *Stk25* knock-down neurons (Fig. 3*E–G*). In addition, MST3 WT and kinase-inactive form of MST3 overexpression caused the formation of multiple axons in cultured neurons (Fig. 3*G*), consistent with what we previously observed in *Stk25* knock-down neurons overexpressing STK25 (Matsuki et al., 2010). Based on these findings, we investigated whether *Mst3* knock-down would affect axonogenesis, and whether STK25 would compensate for *Mst3* knock-down. As with *Stk25* knock-down, *Mst3* knock-down resulted in reduced axonogenesis and consequently the length of the longest process (Fig. 3*K*,*O*). This was rescued by both STK25 WT and kinase-inactive form of STK25 overexpression (Fig. 3*L–O*).

We previously reported STK25 regulates intestinal and neuronal cell polarization downstream of LKB1 (Matsuki et al., 2010). Therefore, we examined whether MST3 can compensate for STK25 downstream of LKB1 and vice versa whether STK25 can compensate for loss of MST3, in cell polarization. Knock-down of LKB1 in mouse neurons by *in utero* electroporation with an *Lkb1* shRNA expressing plasmid led to loss of axon formation (Fig. 4*A*,*B*), consistent with what has been observed previously (Barnes et al., 2007; Shelly et al., 2007). Combined knock-down of *Lkb1* and *Mst3* and *Lkb1* and *Stk25* also lead to reduced neuronal polarization as compared with the control but these further manipulations did not augment the polarization defect compared with *Lkb1* knock-down alone. We then assessed whether STK25 expression was capable of rescuing the combined knock-down of *Lkb1* and *Mst3* by adding a STK25 expressing

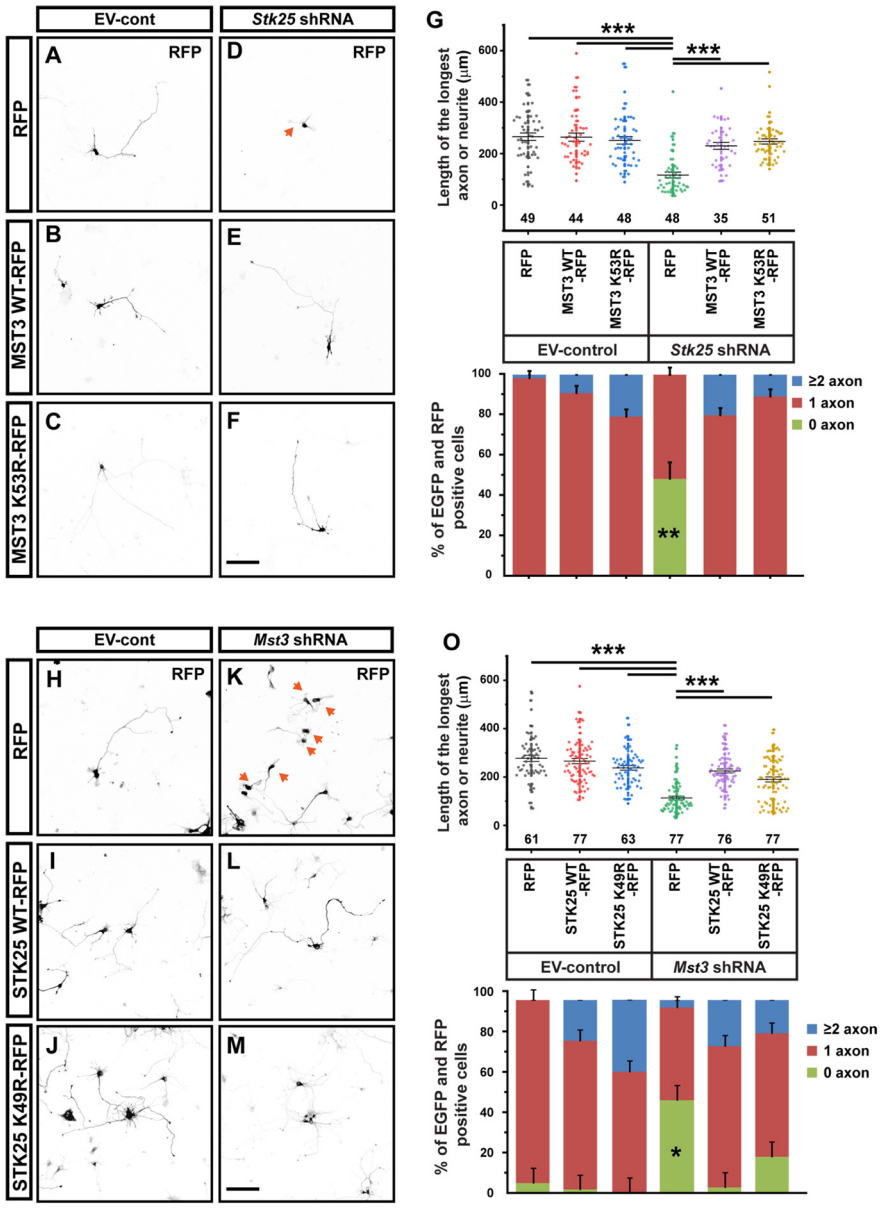

Figure 3. MST3-RFP expression rescues neuronal polarization defects caused by *Stk25* knock-down in cultured neurons. ***A***, ***H***, Neurons expressing RFP alone with the control virus (EV-cont). ***B***, ***C***, Neurons overexpressing MST3 WT-RFP or MST3 K53R-RFP. ***D***, *Stk25* knock-down neurons co-expressing RFP lacked an axon or had a much shorter process, as compared with controls (orange arrow). ***E***, ***F***, Neurons overexpressing MST3 WT-RFP or MST3 K53R-RFP with *Stk25* knock-down. ***G***, Quantitative analysis of the length of the longest process and the percentage of cells that are polarized and extend axons identified with axonal marker SMI-312 (images are not shown) from ***A–F***. The number below each dataset represents the number of analyzed neurons. Each dot represents the data of an individual neuron. The lower graph shows the ratios of neurons with 0, 1, and >2 axons, respectively, in percentage among total analyzed neurons expressing both GFP and RFP. ***I***, ***J***, Neurons overexpressing of STK25 WT-RFP or STK25 K49R-RFP. ***K***, *Mst3* knock-down inhibited axon formation and/or led to formation of shorter processes in neurons (orange arrows). ***L***, ***M***, Neurons overexpressing STK25 WT-RFP and K49R-RFP with *Mst3* knock-down. ***O***, Quantification of length of the longest process and percentage of neurons producing SMI-312-positive axons from ***H–M***. The number below each dataset represents the number of analyzed neurons. Each data point represents the process length of an individual neuron. The lower graph shows the ratios of neurons with 0, 1, and >2 axons, respectively, in percentage among total analyzed neurons expressing both GFP and RFP (***$p < 0.001$, one-way ANOVA with Holm–Bonferroni *post hoc* test; $n \geq 3$; error bars, SEM; scale bars: 100 μm).

plasmid to the *in utero* electroporation. We found that both STK25 WT and KI very effectively rescued the loss of polarization resulting from loss of LKB1 and MST3. To examine whether MST3 expression could rescue the combined loss of LKB1 and STK25, we overexpressed STK25 in *Mst3*/*Lkb1* knock-down brains. MST3 also rescued in a kinase independent manner.

We next turned to intestinal epithelial cells, the polarization of which has been shown to be regulated by LKB1/STRADα signaling and STK25 (Baas et al., 2004; Matsuki et al., 2010). This has been convincingly shown with an epithelial line, W4, which has been modified to constitutively express LKB1 and inducibly express the pseudokinase STRADα in response to Dox (Baas et al., 2004). STRADα expression stabilizes LKB1 protein and leads to polarized formation of the brush border. Reducing the endogenous *STK25* suppresses cell polarization following Dox induction of STRADα (Matsuki et al., 2010; Fig. 4*E*,*F*). To determine whether endogenous MST3 expression is also required for LKB1-STRADα-induced polarization, we generated *MST3* shRNA vectors effective at reducing endogenous expression in human cells (Fig. 4*G*). We examined whether MST3 also acts downstream of LKB1 during cell polarization or not. We found that *MST3* knock-down in W4 cells hindered brush border formation in response to Dox treatment (Fig. 4*C*,*D*). We observed that overexpressing MST3 rescued brush border formation in *MST3*-knock-down W4 cells (Fig. 4*C*,*D*), similar to the rescue of brush border formation in *STK25* knock-down W4 cells by overexpressing STK25 (Matsuki et al., 2010; Fig. 4*E*,*F*). We also found that both STK25 WT and kinase-inactive form of STK25 rescued cell polarization in *MST3* knock-down W4 cells (Fig. 4*C*,*D*). Similarly, we revealed that overexpressing MST3 in *STK25* knock-down cells rescued cell polarization in a kinase activity-independent manner (Fig. 4*E*,*F*). Together, it appears that the kinase activities of neither STK25 nor MST3 are required to regulate polarization of epithelial cells or neurons, and that a different feature of these proteins such as their role in protein scaffolding is required.

Reducing STK25 expression leads to compensatory upregulation in MST3 and vice versa

STK25 and MST3's overlapping roles in the regulation of neuronal migration and polarization suggests that they have compensatory roles for each other during cortical development under certain circumstances. Expression of STK25 can be acutely reduced in *Stk25*$^{fl/fl}$ mice expressing Cre-ER^{TM}, a tamoxifen inducible version of Cre, by exposing the embryos to tamoxifen, which we did at E14.5. Stk25 expression was no longer detectable 2 d later, but MST3 expression was not significantly

altered as compared with *Stk25*$^{fl/fl}$ mice lacking the *Cre-ER*^{TM} gene, suggesting that genetic compensation had not occurred (Fig. 5*A*,*B*). Since this may not be sufficient time for compensation to occur, we checked again at E18.5. As expected, STK25 protein levels were dramatically reduced (Fig. 5*A*,*C*). In contrast to the finding at E16.5, MST3 proteins were more highly expressed by ~30% than those in the genetic controls lacking Cre-ER^{TM} expression (Fig. 5*C*,*D*). Interestingly *Mst3* mRNA levels were indistinguishable between the cKO mice and the control (Fig. 5*E*), suggesting that the difference of MST3 protein levels is because of a post-transcriptional mechanism.

To investigate whether compensatory upregulation of STK25 might also take place or not in conditions of disturbed MST3 expression, we knocked down *Mst3* in cultured embryonic neurons using a lentivirus that expresses an *Mst3* shRNA. Infection was done on the second day in culture and protein expression was analyzed 4 d later. *Mst3* shRNA expression effectively reduced MST3 protein expression, and STK25 proteins were more abundantly expressed by ~60% than those in the control (Fig. 5*F*, *G*). To determine whether this expressional compensation between STK25 and MST3 are relevant in migrating neurons *in vivo*, we transfected the Cre-expressing plasmid into *Stk25*$^{fl/fl}$ embryos and the *Mst3* shRNA-expressing plasmid into *WT* embryos at E14.5 and analyzed immunoreactive signals at E17.5. These analyses demonstrated that MST3 protein was more highly expressed in GFP (+), *Stk25*-deficient neurons in the cortical plate, than in nearby untransfected neurons (Fig. 5*H*,*J*). Similarly, STK25 protein expression was more abundant in *Mst3* knock-down neurons as compared with the adjacent untransfected neurons (Fig. 5*H*,*I*). The upregulation of STK25 and MST3 only was observed in the cortical plate and not in neurons in the intermediate zone or VZ.

As discussed above, suppressing *Stk25* gene function at E14.5, did not lead to increased MST3 expression by E16.5 (Fig. 5*A*); however, we observed increased expression by E18.5 (Fig. 5*C*,*D*). This begs the question whether the compensation was too slow to prevent anomalous neuronal migration within 3 d after knock-down or KO of the GCKIII kinases. To examine this further, we conditionally knocked out *Stk25* in *Stk25*$^{fl/fl}$; *Cre-ER*^{TM} mice by tamoxifen injections at E10.5 and compared the cortical phenotype to

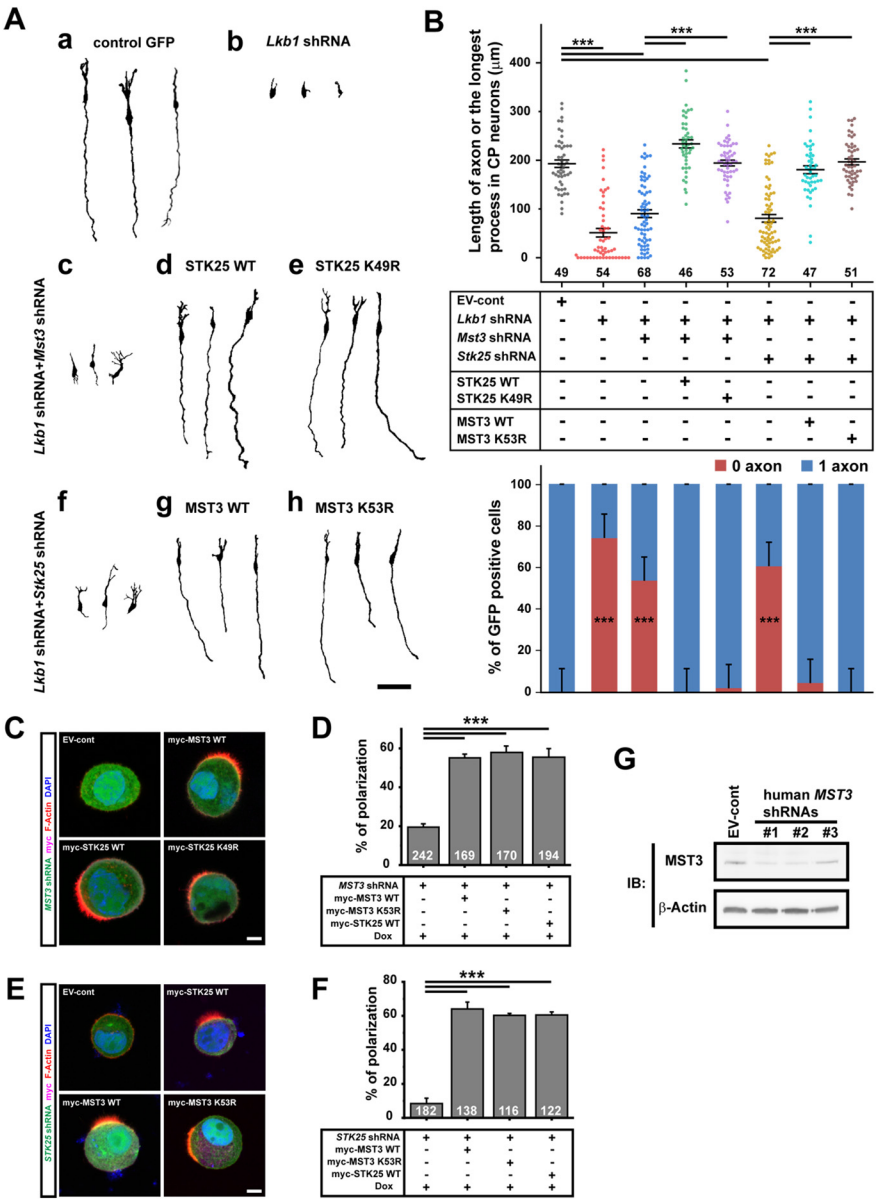

Figure 4. Evaluation of the roles of STK25 and MST3 in the LKB1 pathway. ***A***, ***a–h***, Computer-based reconstructed images represent typical neurons from the cortical plate of WT mice at E17.5 after *in utero* electroporated at E14.5 with the plasmids indicated on the vertical and horizontal axes. Scale bar: 50 μm. ***B***, Upper panel represents the quantitative analysis of the length of the longest process for cortical plate (CP) neurons, each data are represented by a single dot. Each basal process longer than 90 μm was regarded as an axon in the graph below that shows the percentage of axon possessing and lacking neurons. The axon-initiation defect caused by knock-down of *Lkb1* and either *Mst3* or *Stk25* were rescued by overexpression of the other GCKIII kinase in an activity-independent manner. The numbers indicated below each dataset represent the number of neurons analyzed from at least three brains (***$p < 0.001$, one-way ANOVA with Holm–Bonferroni *post hoc* test; error bars, SEM). ***C***, Induction of STRADα expression with Dox treatment failed to induce formation of an actin-rich brush border when MST3 was knocked down (EV-cont, upper left panel). However, myc-MST3 WT expression (upper right) rescued cell polarization. The *MST3* shRNA-induced cell polarization deficit was also rescued by overexpression of STK25, independent of kinase activity (lower left and right panels). ***D***, Quantitative analysis of the W4 cell polarization shown in ***B***. The number below each bar represents the number of cells analyzed from three independent experiments (***$p < 0.001$, one-way ANOVA with Holm–Bonferroni *post hoc* test). ***E***, Similar to polarization rescue by myc-STK25 in *MST3* knock-down cells, overexpression of myc-MST3 rescued the cell polarization independent of kinase activity in *STK25* knock-down cells (lower right and left panels). ***F***, Quantitative analysis of the W4 cell polarization shown in ***E***. The number below each bar represents the total number of cells analyzed (***$p < 0.001$ one-way ANOVA with Holm–Bonferroni *post hoc* test; $n = 3$; error bars, SEM). ***G***, Validation of the knock-down efficiency of human MST3. The shRNA #1 and #2 showed the greatest reduction of endogenous MST3 expression in W4 cells and we used shRNA #1 here. Scale bars in ***C***, ***E***, lower right panels: 5 μm.

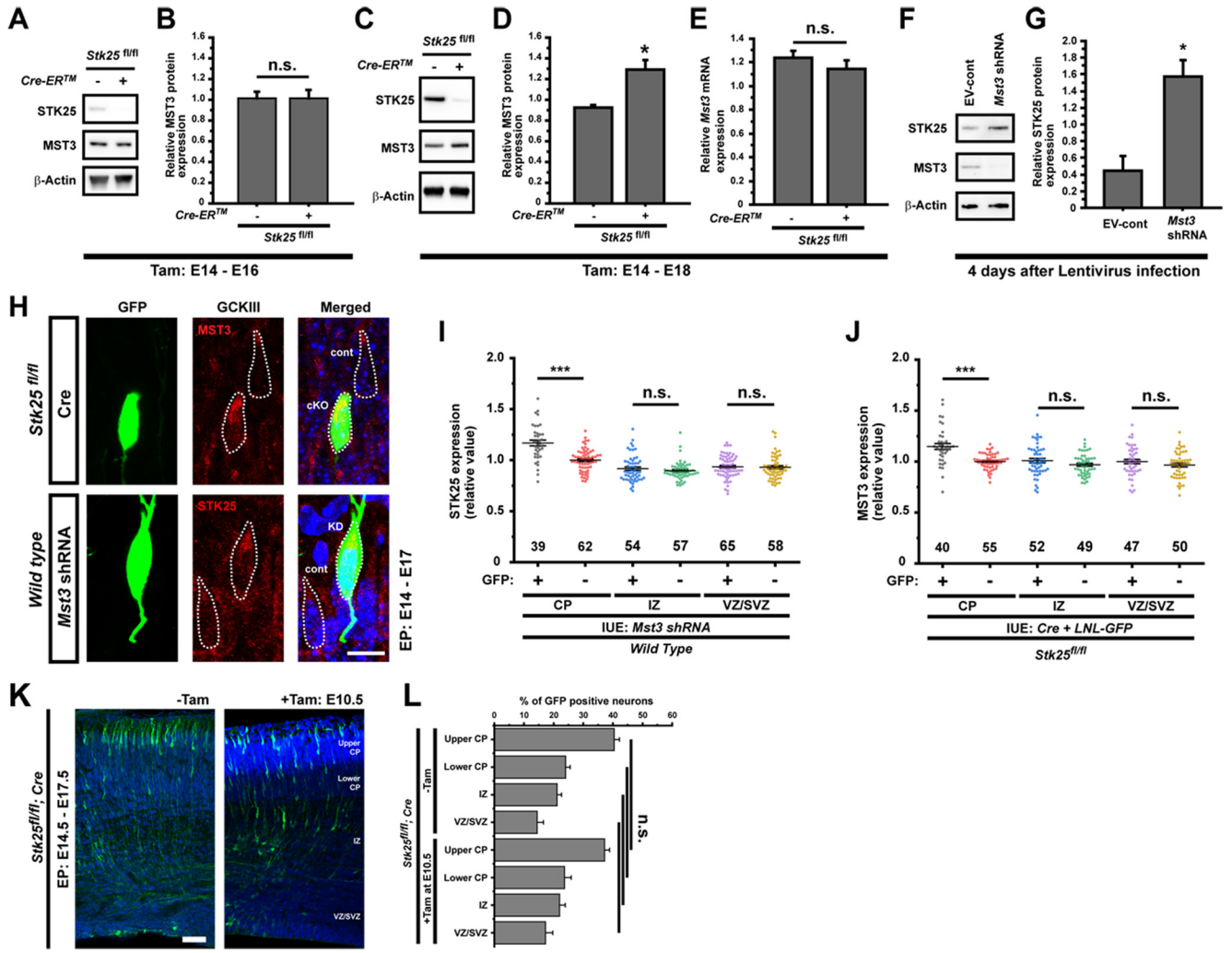

Figure 5. Compensatory responses in STK25 and MST3 protein expression. ***A***, ***B***, Immunoblot analysis showed no difference in MST3 protein expression between *Stk25*$^{fl/fl}$ embryos with *Cre-ER*^{TM} and *Stk25*$^{fl/fl}$ embryos without *Cre-ER*^{TM}. Both were treated with tamoxifen at E14.5 to activate Cre and killed at E16.5 (n.s., not significant; Student's *t* test, $n = 4$). ***C***, ***D***, Immunoblot analysis demonstrated upregulated MST3 protein expression in *Stk25*$^{fl/fl}$ embryos with Cre-ER^{TM} compared with *Stk25*$^{fl/fl}$ embryos without Cre-ER^{TM}. Both were treated with tamoxifen at E14.5 to activate Cre, when present and killed at E18.5 (*$p < 0.05$, Student's *t* test, $n = 3$; error bars, SEM). ***E***, qPCR analysis from triplicate experiments demonstrated no significant difference in *Mst3* mRNA expression in *Stk25*$^{fl/fl}$ embryos with/without Cre-ER^{TM}, treated with tamoxifen as described above (n.s., not significant; Student's *t* test, $n = 3$). ***F***, ***G***, *Mst3* knock-down led to elevated STK25 protein in cultured neurons (*$p < 0.05$, Student's *t* test, $n = 4$; error bars, SEM). ***H***, Immunohistochemical analysis of MST3 levels in *Stk25* cKO neurons and STK25 levels in *Mst3* knock-down neurons located in the cortical plate 3 d after *in utero* electroporation at E14.5 (scale bar: 10 μm). ***I***, ***J***, Quantitative analysis of indicated immunofluorescent signals (*y*-axis) in each layer for GFP expressing GCKIII kinase-deficient cells (*Mst3* deficient in ***I*** and *Stk25* deficient in ***J***) as compared with adjacent untransfected cells. The number below each dataset represents the number of neurons analyzed (***$p < 0.001$, n.s., not significant; one-way ANOVA with Holm–Bonferroni *post hoc* test; $n = 3$; error bars, SEM). ***K***, When *Stk25* was inactivated in *Stk25*$^{fl/fl}$; *Cre-ER*^{TM} embryos by tamoxifen injection at E10.5 (right panel), the majority of GFP^{+} neurons labeled by *in utero* electroporation at E14.5 migrated into the cortical plate by E17.5, similar to the uninjected-control sample (left). ***L***, Quantification of the GFP+ neurons in the cortical layers of E17.5 *Stk25*$^{fl/fl}$; *Cre-ER*^{TM} embryos as shown in ***K*** (n.s., not significant; one-way ANOVA with Holm–Bonferroni *post hoc* test; $n = 4$; error bars, SEM; CP, cortical plate; IZ, intermediate zone; VZ/SVZ, ventricular zone and subventricular zone).

uninjected controls. To visualize the same class of neurons in the earlier experiments, we electroporated the control GFP expressing plasmids into cortices at E14.5 and analyzed the position of the GFP^{+} neurons at E17.5. Under these conditions, the percentages of GFP^{+} neurons in the same layer between control and *Stk25* cKO animals were very similar (Fig. 5*K*,*L*), suggesting that if gene activation occurs early enough there is sufficient time for compensation to occur and prevent a migration phenotype.

Rac1 regulates neuronal migration downstream of STK25

Recently, it has been reported that MST3 promotes neuronal migration by regulating RhoA (Tang et al., 2014). Since other Rho GTPase family members are also important regulators of neuronal migration, we wondered whether Rac1 and Cdc42, in addition to RhoA, might be involved in signaling pathways downstream of the GCKIII family kinases (Kawauchi, 2015; Lawson and Ridley, 2018). We examined the interaction of these Rho GTPases with STK25 and MST3 by co-IP from cell lysates of transiently transfected HEK293FT cells. Both STK25 and MST3 were co-IP robustly with Rac1 (Fig. 6*A*). Cdc42 also interacts with the GCKIII kinases, however, the co-IP efficiency was lower than that observed between Rac1 and the GCKIII kinases and a longer exposure was required to visualize the associated protein although inputs were comparable (Fig. 6*A*). In contrast, RhoA levels seem to be reduced by GCKIII expression making it difficult to assess an interaction (Fig. 6*A*).

Since Rac1 showed the most robust co-IP with STK25, we addressed whether it plays a role in STK25-regulated neuronal migration. Accordingly, we examined Rac1's possible roles in neuronal migration by determining whether it was capable of

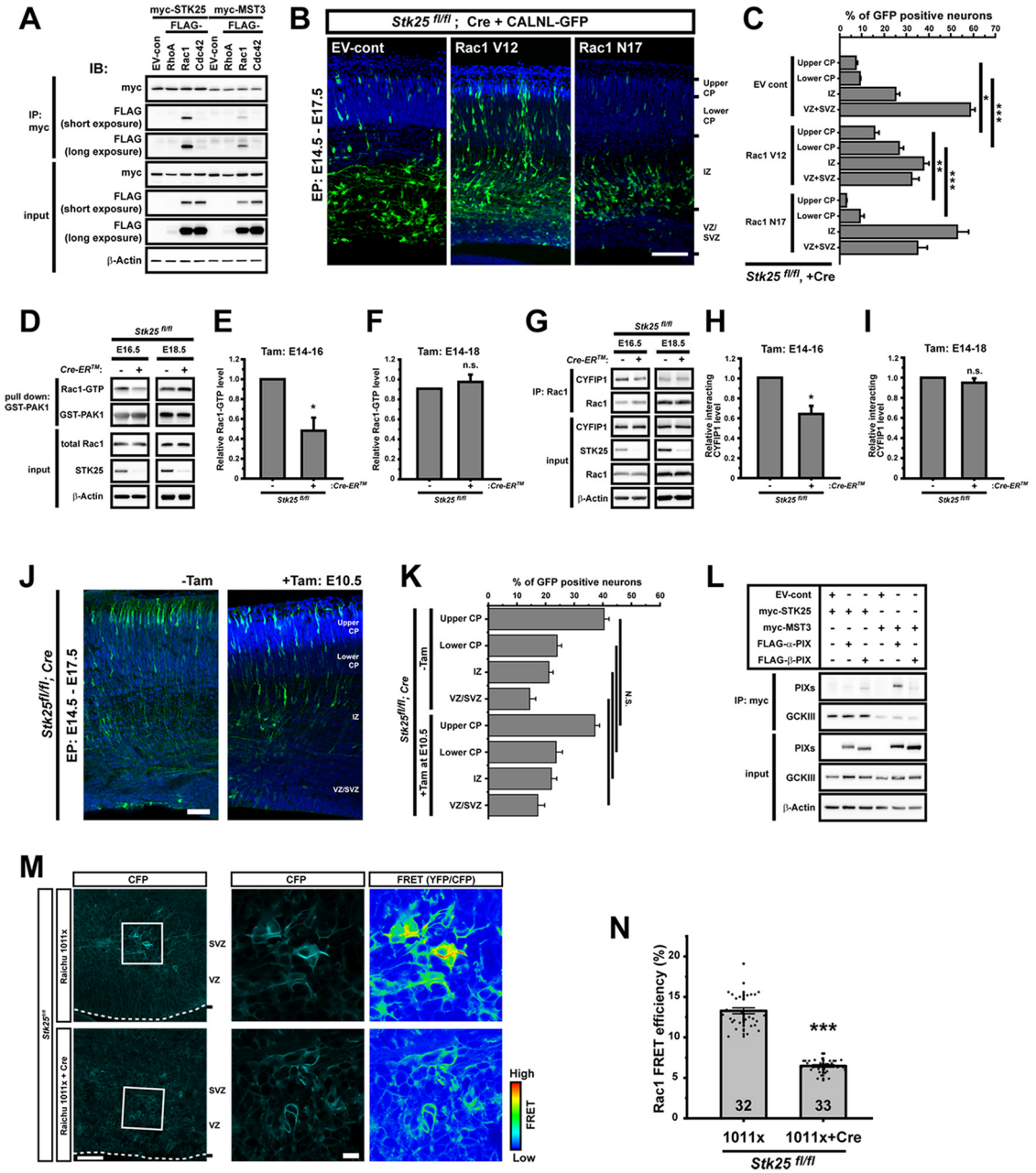

Figure 6. Rac1 forms a complex with and acts downstream of STK25 during neuronal migration. ***A***, The interaction between GCKIII proteins and Rac1 seemed much stronger than that between GCKIIIs and Cdc42. (first and second panels from top). ***B***, ***C***, There was a larger population of GFP$^+$ neurons entering the cortical plate in the Rac1 V12 than EV-cont or Rac1 N17 transfected with indicated vectors in *Stk25$^{fl/fl}$* brains. (*$p < 0.05$, **$p < 0.01$, ***$p < 0.001$, one-way ANOVA with Holm-Bonferroni *post-hoc* test; $n \geq 3$; Error bars, SEM; cortical plate, CP; intermediate zone, IZ; ventricular/subventricular zones, VZ/SVZ). ***D***, Stk25 cKO at E14.5 suppressed Rac1 activation in lysates from the developing cortex at E16.5 (shown in left panels); however, Rac1-GTP recovered to the control level at E18.5 (right panels). ***E***, ***F***, Quantitative analysis of the Rac1-GTP levels shown in ***D*** at E16.5 and E18.5, respectively (*$p < 0.05$, Student's *t* test, $n \geq 3$). ***G***, Stk25 cKO at E14.5 resulted in a decreased amount of CYFIP1 that co-immunoprecipitated with Rac1 at E16.5 as compared to the control (left top panel), but by E18.5 there was no difference between the two (right top panel). ***H***, ***I***, Quantitative analysis of the CYFIP1-Rac1 co-immunoprecipitation at E16.5 and E18.5 from ***G***, respectively (*$p < 0.05$, n.s., not significant. Student's t test, $n = 3$). ***J***, *Stk25$^{fl/fl}$;Cre-ER^{TM}* mice with or without Tamoxifen exposure at E10.5, electroporated GFP plasmids at E14.5 and analyzed at E17.5 displayed no significant difference in neuronal migration. ***K***, Quantification of the population of GFP+ neurons in the cortical layers of E17.5 *Stk25$^{fl/fl}$;Cre-ER^{TM}* embryos from J. (N.S., not significant. one-way ANOVA with Holm-Bonferroni post-hoc test; $n \geq 3$; Error bars, SEM; cortical plate, CP; intermediate zone, IZ; ventricular/subventricular zones, VZ/SVZ). ***L***, Both STK25 and MST3 interact with a- and b-PIX. We immunoprecipitated either myc-STK25 or myc-MST3 and assayed for co-purification of FLAG-tagged a- or b-PIX by immuno-blotting (upper panel) from the lysates of the indicated combinations of HEK293FT cell transfections. ***M***, In vivo FRET analysis of Rac1 activity on *Stk25$^{fl/fl}$* mouse cortices transfected with the indicated plasmids. The left panels show the CFP signal (Scale bar, 50 mm). The middle and right panels represent the CFP signal and FRET ratio in the boxed region (Scale bar, 10 mm). ***N***, Quantification of FRET efficiency is shown in ***C*** (***$p < 0.001$, Student's *t* test; Error bars, SEM; $n \geq 3$ animals). The number in each bar shows the number of analyzed neurons.

rescuing the position defect in *Stk25* cKO neurons, which we observed previously (Matsuki et al., 2013). Co- electroporation of dominant active Rac1 V12 along with Cre and the Cre-reporter GFP vector CALNL-GFP, into *Stk25$^{fl/fl}$* E14.5 embryos improved neuronal migration into the upper and lower cortical plate as compared with no exogenous Rac1 expression (EV-cont; Fig. 6*B*,*C*). In contrast, co-electroporation of dominant negative Rac1 N17 with Cre and CALNL-GFP did not

rescue neuronal migration defects caused by reduced *Stk25* (Fig. 6*B*,*C*), suggesting that Rac1 may act downstream of STK25.

To determine whether and how STK25 might regulate Rac1 activity, we measured Rac1-GTP levels in cortices of mouse brains where *Stk25* was conditionally disrupted at E14.5. These *Stk25*$^{fl/fl}$ mice also carried the *Cre-ER*^{TM} transgene, which efficiently inactivated the floxed *Stk25* gene in response to tamoxifen (Fig. 6*D*). Active Rac1 levels were determined by Western blotting the GST-PAK1 effector-domain-purified fraction of brain lysates from *Stk25 cKO* and control mice, lacking *Cre-ER*^{TM}. GST-PAK1-bound Rac1-GTP levels were downregulated in *Stk25*-deficient mice compared with the control at E16.5 (Fig. 6*D*,*E*). However, the active Rac1 level in *Stk25 cKO* mice recovered to the control level by E18.5 (Fig. 6*D*,*F*). To explore the upstream mechanism, we focused on the guanine nucleotide exchange factors (GEFs) α-PIX and β-PIX as possible Rac1 regulators. Both are well-known GEFs of the Rho GTPase family and are involved in cell migration (Baird et al., 2005; ten Klooster et al., 2006). We examined whether these GEFs form complexes with STK25 and/or MST3 in HEK293FT cells. Both STK25 and MST3 were co-IP with α-PIX and β-PIX (Fig. 6*J*), suggesting a possible mechanism, whereby STK25 and potentially MST3 regulate the Rac1 axis to influence neuronal positioning.

Next, we tested the interaction intensity between Rac1 and cytoplasmic FMR1 interacting protein 1 (CYFIP1), a member of the WAVE complex, that is known to be involved in actin remodeling through the interaction with activated Rac1 (Steffen et al., 2004; Anitei et al., 2010; Tahirovic et al., 2010; Fan et al., 2018; Schaks et al., 2018). The CYFIP1 interaction with Rac1 reflected the Rac1-GTP level ascertained by the GST-PAK1 effector domain interaction, suggesting that this interaction is Rac1 activation state dependent (Fig. 6*G*–*I*). This result provides a potential direct link between the STK25-Rac1 signaling pathway and the regulation of actin polymerization.

To determine whether STK25 regulates Rac1 activation in migrating neurons during development, we co-electroporated a Rac1 biosensor, with or without Cre, into the developing neocortex of *Stk25*$^{fl/fl}$ mice. To assay Rac1 activity, we used the Raichu 1011× Rac1 biosensor that undergoes FRET when Rac1 is in the GTP bound state because of an intramolecular interaction with Pak that aligns the CFP and the YFP domains (Itoh et al., 2002). The FRET signal was highest in the SVZs of the Cre (–) control cortices. In contrast, the FRET signal intensity in the same region of brains cotransfected with Cre was approximately half of that in the control (Fig. 6*K*,*L*). These results indicated Rac1 activation in developing neurons is dependent on STK25 expression and consistent with a role for STK25 in the SVZ.

STK25 and MST3 regulate RhoA stability

MST3 was previously shown to interact with RhoA and regulate its phosphorylation at serine 26, an inhibitory site for RhoA's activity (Tang et al., 2014). In addition, RhoA knock-down was shown to rescue neuronal position defects caused by *Mst3* shRNA expression. We observed a reduced RhoA expression in cells expressing the GCKIII kinases (Fig. 6*A*), which potentially suggests a different mode of regulation from the one previously reported. To address this issue further, we assayed RhoA levels in HEK293FT cells co-transfected with increasing amounts of STK25 or MST3. Interestingly, RhoA protein levels had an inverse correlation with the expression levels of STK25 and MST3 kinases (Fig. 7*A*,*B*). To determine whether the suppression of RhoA levels by the GCKIIIs was caused by accelerated protein degradation, we analyzed the effects of proteasome and lysosomal degradation inhibitors. STK25-expressing cells treated with MG132, a proteasome inhibitor, showed elevated RhoA protein expression by 6 h after drug treatment; however, this drug was not effective in MST3-expressing cells even by 24 h after treatment (Fig. 7*C*,*D*). Administration of the lysosomal inhibitor chloroquine (CQ) increased RhoA expression by 6 h after the treatment in both STK25-expressing and MST3-expressing cells (Fig. 7*C*,*D*). These results suggested the possibility that STK25 and MST3 promote the lysosomal degradation of RhoA and that STK25 additionally promotes its proteasomal degradation. Previous studies have reported that some Cullin (Cul) E3 ubiquitin ligase family proteins are involved in neuronal migration (Simó and Cooper, 2013). In addition, Cul3 targets RhoA for degradation via the ubiquitin/proteasome system (Nethe and Hordijk, 2010). We therefore examined the possibility that the GCKIII molecules interact with Cul family members. Interaction assays using HA-tagged STK25 and MST3 with myc-tagged Culs revealed that both STK25 and MST3 associate with Cul1, Cul3, Cul4A, and Cul4B (Fig. 7*E*). In contrast, Cul2, Cul5, and Cul7 interacted with neither STK25 nor MST3. Given the results from MG132 and CQ treatment experiments, we tested whether the interaction of STK25 with Cullin family members regulates RhoA stability. To address whether STK25-Cul complexes target RhoA to the proteasome, we examined RhoA ubiquitination by treatment with MG132 to protect it from degradation. As shown in Figure 7*F*, co-overexpression of STK25 led to reduced RhoA expression as compared with the EV-cont (see FLAG input, left five lanes vs right five lanes). In the IP samples, RhoA levels looked more close suggesting that the amount of antibody used was not saturating, resulting in a partial normalization of the RhoA levels. Cul3 expression leads to lower levels of RhoA especially in the presence of STK25 overexpression (see input for FLAG). MG132 treatment in this experiment stabilized RhoA, as compared with Figure 6*A*, permitting us to assess protein-protein interactions. By co-IP, we detected an interaction between STK25 and RhoA (Fig. 7*F*) that was not dependent on co-overexpression of Cul, which is reminiscent of the interaction observed between MST3 and RhoA previously reported (Tang et al., 2014). We also detected the co-IP of Cullins 1, 3, 4A, and 4B. The amount of IP material was enhanced by co-expression of Stk25 despite a reduction in the level of amount of the IP-target protein FLAG-tagged RhoA. These results suggest that the STK25 interaction with RhoA has an important role in its degradation possibly by enhancing the association with Culs and augmenting RhoA's ubiquitination.

We further explored other complex components, including the E3 ubiquitin ligase complex, which is required for RhoA-specific degradation by the ubiquitin/proteasome system. Possible candidate molecules included Bacurd1/KCTD13 and Bacurd2/TNFIP. Bacurd1 and Bacurd2 are known to be involved in RhoA degradation through forming complexes with Cul3 (Chen et al., 2009). Furthermore, Bacurd1 is involved in neuronal development and related diseases (Lin et al., 2015; Gladwyn-Ng et al., 2016; Escamilla et al., 2017). Co-IP assays between HA-STK25 and myc-tagged Bacurds revealed that both Bacurds were able to form complexes with STK25 (Fig. 7*I*), suggesting that they may be involved in the RhoA degradation that is accelerated by STK25 (Fig. 7*G*,*H*).

RhoA expression in the developing brain is modulated by STK25

Several studies have reported that RhoA expression and/or signaling plays multiple roles in neuronal migration (Kholmanskikh et al., 2003; Pacary et al., 2011; Tang et al., 2014; Xu et al., 2015). However, RhoA's precise roles have not been completely resolved. Our results obtained from cultured cells suggest the potential importance of RhoA stability in neuronal migration. The destabilization of RhoA by STK25 overexpression prompt us to determine whether endogenous RhoA expression levels were affected by *Stk25* cKO. To determine the effect of STK25 on RhoA *in vivo*, we treated $Stk25^{fl/fl}$ and $Cre\text{-}ER^{TM}$ mutant mice with tamoxifen at E14.5 and collected brains for analysis 1 or 2 d later, as indicated in the figure legends. Immunoblot analysis revealed that RhoA expression was upregulated in $Stk25^{fl/fl}$ mice expressing $Cre\text{-}ER^{TM}$ as compared with Cre-negative littermates (Fig. 8*D*,*E*). Immunohistological staining revealed that RhoA-immunoreactive neurons had a greater likelihood of being in the VZ and a smaller likelihood of being in the intermediate zone in the *Stk25*-deficient neurons as compared with controls 1 d after tamoxifen treatment (Fig. 8*A*,*B*). Thus, we examined the relative intensity of RhoA fluorescent immunosignals between tamoxifen-exposed $Stk25^{fl/fl}$ mice expressing $Cre\text{-}ER^{TM}$ and the Cre-negative littermate control. Endogenous RhoA expression was upregulated in *Stk25*-deficient neurons (Fig. 8*B*,*C*) and this was reflected in the immunoblot analysis of the whole cortex (Fig. 8*D*,*E*). Collectively, these findings suggest that STK25 keeps RhoA levels low, which accelerates neuronal migration.

Rac1 activation and RhoA suppression act synergistically to rescue neuronal migration defects caused by *Stk25* deficiency

With the evidence that STK25 both upregulates Rac1 activity and downregulates RhoA levels, we investigated whether knocking down RhoA, alone or in conjunction with overexpressing Rac1 V12, could rescue the migration defect in *Stk25*-deficient brains. We co-introduced Cre, the Cre reporter CALNL-GFP, and plasmids expressing *RhoA* shRNA into $Stk25^{fl/fl}$ embryos at E14.5 by *in utero* electroporation (Fig. 9*A*,*B*). *RhoA* knock-down alone did not rescue the neuronal migration defect in Cre-expressing neurons when compared with the control (Fig. 9*A*,*B*). In contrast, Rac1 V12 expression alone improved migration to the lower cortical plate (Figs. 6*B*,*C*, 9*A*,*B*). Next, we investigated whether *RhoA* knock-down and Rac1 V12 expression might act synergistically, by doing a multiplex transfection that included Cre, RacV12, and *RhoA* knock-down plasmids in the $Stk25^{fl/fl}$ embryos. Interestingly knocking down *RhoA* in conjunction with Rac1 V12 expression did lead to robust improvement of neuronal migration of *Stk25*-deficient neurons to both the upper and lower cortical plate, which was superior to Rac1 V12 and *RhoA* shRNA electroporations alone (Fig. 9*A*,*B*). This suggests that STK25's functions to activate Rac1 and to target RhoA for

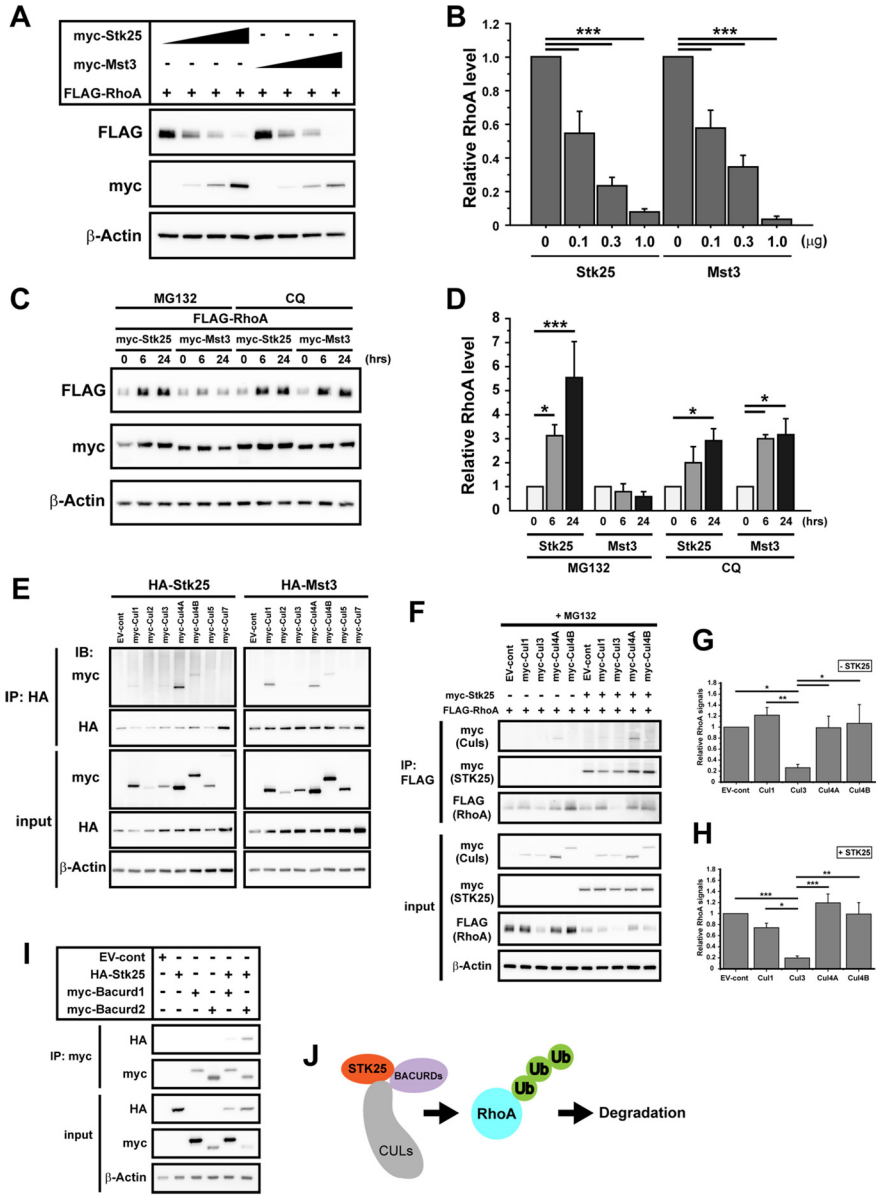

Figure 7. GCKIIIs regulate RhoA stability. ***A***, RhoA expression levels were inversely correlated with the amounts of GCKIII plasmids transfected and GCKIII kinase expressed. ***B***, Quantitative analysis of RhoA expression as shown in ***A***. Amounts of indicated plasmids are shown below graph (0, 0.1, 0.3, 1.0 μg) with a constant amount of RhoA plasmid (1.0 μg) per transfection (***$p < 0.001$, one-way ANOVA with Holm–Bonferroni *post hoc* test; $n = 3$; error bars, SEM). ***C***, RhoA protein levels in GCKIII co-expressing cells at 0, 6, and 24 h after administration of proteasome (MG-132) and lysosome (CQ) inhibitor. ***D***, Quantitative analysis of RhoA expression shown in ***C*** (*$p < 0.05$, ***$p < 0.001$, one-way ANOVA with Holm–Bonferroni *post hoc* test; $n = 3$; error bars, SEM). ***E***, The interaction of Cullins with HA-STK25 and HA-MST3. ***F***, RhoA associates with STK25 and Culs. The amount of co-IP STK25 did not depend on co-overexpression of Culs. In contrast, Culs co-immunoprepicitation was enhanced by co-overexpression of STK25. ***G***, ***H***, The quantitative analysis of RhoA expression in total cell lysate without STK25 expression (FLAG input, five left lanes in ***F***) and with STK25 expression (FLAG input, five right lanes in ***F***; *$p < 0.05$, **$p < 0.01$, ***$p < 0.001$, one-way ANOVA with Holm–Bonferroni *post hoc* test; $n = 3$; error bars, SEM). ***I***, HA-STK25 co-immunoprecipitated with both Bacurd1 and Bacurd2. ***J***, Model for RhoA destabilization by STK25 co-expression.

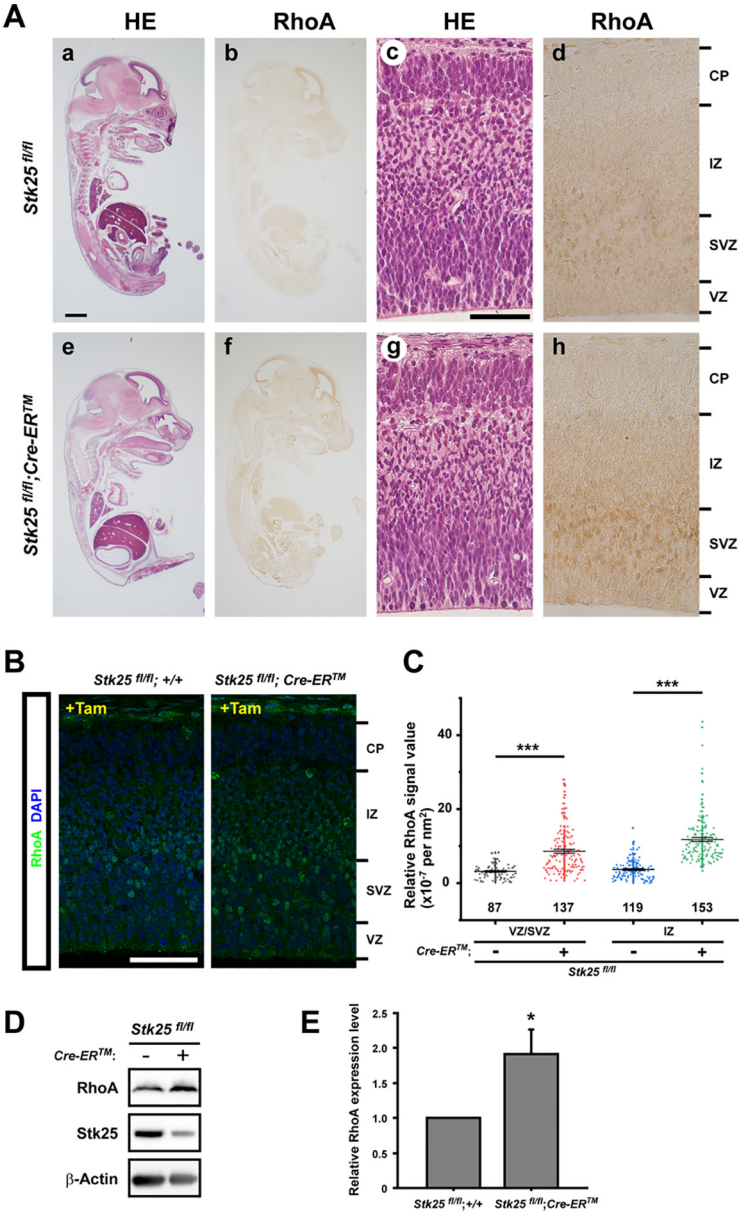

Figure 8. RhoA expression is increased by acute *Stk25* KO. RhoA detection in *Stk25* $^{fl/fl}$ embryos expressing Cre-ER^{TM} or not (as indicated) that were exposed to tamoxifen at E14.5. ***A***, At E15.5 RhoA immunoreactivity is mainly observed between the subventricular zone (SVZ) and intermediate zone (IZ) both in the control *Stk25*$^{fl/fl}$ (***d***) and in *Stk25*-cKO brains (***h***). In contrast to the control, *Stk25*-cKO brains show slightly elevated RhoA immunoreactivity in these areas [***h***; scale bars: 1 mm (***Aa***) and 50 μm (***Ac***)]. ***B***, Similarly, immunofluorescent images from serial sections of the same brains in ***A*** showed increased RhoA expression in the *Stk25*-cKOs. Scale bar: 50 μm. ***C***, Quantitative analysis of immunofluorescent RhoA signals. Each signal was obtained by the selected region of interest (ROI) of RhoA-positive cells in VZ/SVZ and IZ. Then, the relative signal value of ROI was calculated by subtracting the background value from the same unit area. The number shown below each dataset represents the total number of analyzed cells. Data were obtained from three independent brains (***$p < 0.001$, Student's *t* test; $n = 3$; error bars; SEM). ***D***, Increased RhoA expression was also detected in the *Stk25* cKOs, by anti-RhoA immunoblotting of brains from *Stk25*$^{fl/fl}$ with or without *Cre-ER*^{TM}, exposed to tamoxifen at E14.5 and killed at E16.5. ***E***, Quantitative analysis of immunoblot analysis shown in ***D*** (***$p < 0.001$, Student's *t* test; $n = 3$; error bars; SEM).

degradation are both required for optimal regulation of neuronal migration. This is in contrast to knock-down of *Mst3*, which can be rescued simply by knock-down of *RhoA* (Tang et al., 2014).

The ubiquitin ligase complex Baccurd1/Cul3 regulates neuronal migration downstream of STK25

Since the Cullins and Bacurds form complexes with STK25 (Fig. 7*E*,*G*), we investigated whether they could also have effects on anomalous neuronal positioning in *Stk25*-deficient brains. We examined Cul3, 4A, 4B, Bacurd1, and Bacurd2 as candidate regulators of neuronal migration. We introduced a Cre-expression plasmid combined with plasmids carrying cDNA of either Cul3, Cul4A, Cul4B, Bacurd1, or Bacurd2, by *in utero* electroporation as described above. Cul3 and Bacurd1 partially rescued neuronal migration defects caused by inactivation of the *Stk25* gene, whereas Cul4A, Cul4B, and Bacurd2 were ineffective (Fig. 9*C–F*). It was puzzling that both Cul3 and Bacurd1, which are best known to regulate RhoA degradation (Chen et al., 2009; Sailland et al., 2014), effectively rescued migration in *Stk25*-deficient neurons, although RhoA reduction was insufficient to rescue neuronal migration completely (Fig. 9*A–F*). Therefore, we were curious whether Cul3 and Bacurd1 also regulate Rac1 activation. We assayed active Rac1-GTP levels as described above by GST-Pak1 effector domain purification followed by Western blotting. This revealed that Rac1 activation was induced by sole transfection of either Cul3 or Bacurd1 as compared with the vector control, Cul4A, Cul4B, or Bacurd2, in transfected HEK293FT cells (Fig. 9*H*,*I*). Altogether, these data suggest that overexpression of Cul3 or Bacurd1 triggers Rac1 activation in migrating neurons. Immunohistochemical staining showed that Cul3 and Bacurd1 were indeed expressed in the developing cortex at E15.5. The strongest immunoreactivities were observed along the ventricular surface and in VZ (Fig. 10*B*,*D*,*G*,*I*). These results suggest that STK25 acts via a Cul3-Bacurd1 complex to regulate RhoA levels and Rac1 activation during neuronal migration.

Discussion

To explain discrepancies between constitutive and acute *Stk25* loss-of-function phenotypes (Matsuki et al., 2013), we investigated whether related GCKIII kinases might compensate for inactivated *Stk25*. We found that MST3 compensates for STK25 deficits in several processes, including, neuronal migration, axonogenesis, and cell polarization (Figs. 1*D*,*E*, 2*A–C*, 3*A–G*, 4*A*,*B*, 4*E*,*F*). Similarly, STK25 compensates for loss of MST3 (Figs. 1*F*,*G*, 2*D–F*, 3*H–O*, 4*A*,*B*, 4*C*,*D*). In the case of cell polarization these kinases appear to work downstream of LKB1, since knocking down either *Stk25* or *Mst3* blocked LKB1/STRAD-induced intestinal epithelial cell polarization (Fig. 4*C–F*; Matsuki et al., 2010). *Lkb1* deficiency also leads to loss of axonogenesis a hallmark of neuronal polarization (Barnes et al., 2007; Shelly et al., 2007). Here, we found that knock-down of *LKB1* and *Mst3* was rescued by STK25 overexpression and similarly knock-down of *LKB1* and *Stk25* was rescued by MST3 overexpression, suggesting that these kinases act on the LKB1/STRAD pathway for axonal polarization also. MST3 levels

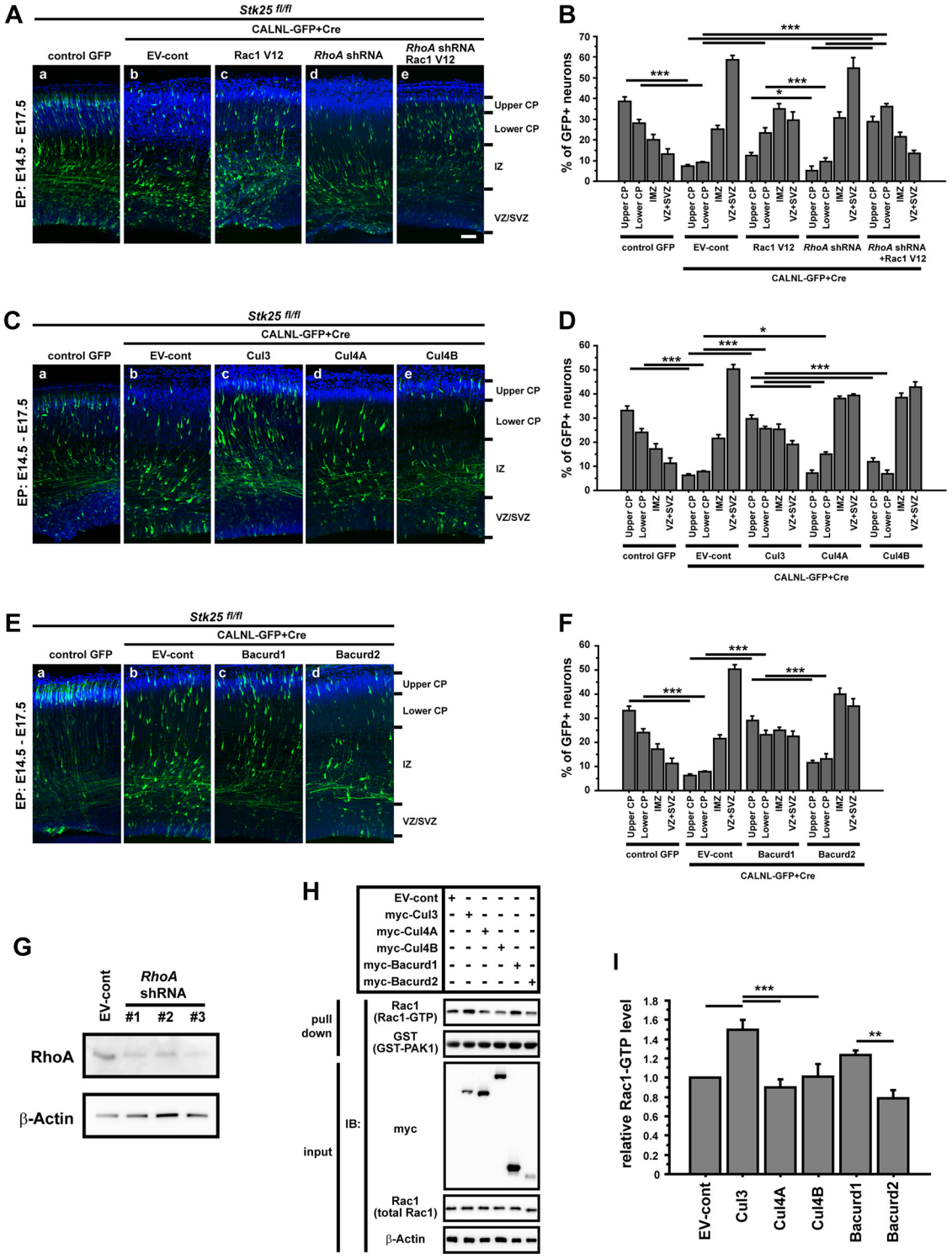

Figure 9. Cul3 and Bacard1 rescue neuronal migration of *Stk25*-deficient neurons similar to combined RhoA depletion and Rac1 activation. ***A***, RhoA knock-down alone is not sufficient to rescue migration of *Stk25*-deficient neurons (***d***), but does so in combination with Rac V12 (***e***). Scale bar: 50 μm. (CP, cortical plate; IZ, intermediate zone; VZ/SVZ, ventricular zone and subventricular zone) ***B***, Quantification of the population of GFP^+ neurons in the cortical layers of E17.5 $Stk25^{fl/fl}$ embryos from ***A***, GFP control from Figure 1*C*, Rac1 V12 from Figure 6*C* ($^*p < 0.05$, $^{***}p < 0.001$; one-way ANOVA with Holm–Bonferroni *post hoc* test; $n \geq 3$ brains; $n \geq 60$ neurons per section). ***C***, Of the tested Cullins, only co-electroporation of Cul3 (***c***) with Cre rescued the neuronal migration of *Stk25*-deficient neurons (***b***). ***D***, Quantification of the population of GFP^+ neurons in the cortical layers of E17.5 $Stk25^{fl/fl}$ embryos. The EV-cont and GFP-control data are from Figures 4*C*, 1*E*, respectively ($^*p < 0.05$, $^{***}p < 0.001$; one-way ANOVA with Holm–Bonferroni *post hoc* test; $n \geq 3$ brains; $n \geq 54$ neurons per section). ***E***, Bacurd1 (***c***) but not Bacurd2 (***d***) overexpression rescued the migration defect. ***F***, Quantification of the population of GFP^+ neurons in the cortical layers of E17.5 $Stk25^{fl/fl}$ embryos from E and GFP control from Figure 1*C* ($^{***}p < 0.001$; one-way ANOVA with Holm–Bonferroni *post hoc* test; $n \geq 3$ brains; $n \geq 105$ neurons per section). ***G***, Assessment of *RhoA* knock-down efficacy. Three shRNA expressing lentiviruses were used to infect 2 DIV hippocampal neurons and analyzed at 6 DIV. Based on its efficacy, we used shRNA #1 for all experiments. ***H***, Overexpression of Cul3 or Bacurd1 lead to elevated endogenous Rac1-GTP levels. ***I***, Quantitative analysis of immunoblotting signals of Rac1-GTP shown in ***G*** ($^{**}p < 0.01$, $^{***}p < 0.001$; one-way ANOVA with Holm–Bonferroni *post hoc* test; $n = 3$; error bars, SEM).

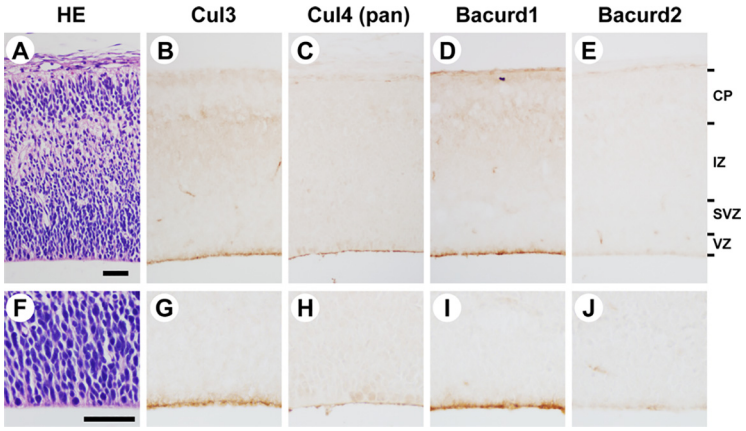

Figure 10. Cul3 and Bacurd1 have similar patterns of immunoreactivity in the developing mouse cortex. Immunohistochemical staining analysis revealed that Cul3 (***B***, ***G***) and Bacurd1 (***D***, ***I***) are expressed in similar locations in the developing neocortex at E15.5. Cul4 (***C***, ***H***; pan antibody) immunostaining pattern was similar to those of Cul3 and Bacurd1, but the intensities were weaker. Bacurd2 immunoreactivity was hardly detectable (***E***, ***J***). An hematoxylin and eosin staining image (***A***) adjacent to sections used in ***B–E***. Higher magnification views of SVZ and VZ are shown in lower panel (***F–J***). Scale bars: 50 μm (***A***, ***F***). CP, cortical plate; IZ, intermediate zone; SVZ, subventricular zone; VZ, ventricular zone.

are upregulated in *Stk25*-deficient mouse brain and vice versa by 3–4 d after the loss of the other kinase (Fig. 5*C*,*D*,*H–J*). While this does not prevent a defect in corticogenesis (Fig. 1*D–F*, EV-cont), disrupting *Stk25* 4 d earlier did not produce phenotypic anomalies when analyzed at E17.5 (Fig. 5*I*,*J*), suggesting that genetic compensation takes several days to be functionally effective. Indeed, we did not detect increased MST3 2 d after *Stk25* gene inactivation and only in a subset of neurons by day 3 (Fig. 5*A*,*B*,*H*,*J*). Since it takes time for genetic compensation to function it appears neurons are dependent on Stk25 function around E14.5 but not around E10.5. Like STK25, MST3 is required for LKB1/STRADα-induced axonal formation and polarization of intestinal epithelial cells suggesting that it acts downstream of LKB1 in some contexts (Fig. 4*A–D*). It had previously been shown that MST3 inhibits RhoA activity, thus we investigated whether STK25 regulates the Rho GTPases. We found that STK25 activates Rac1 (Fig. 6*D*,*E*,*K*,*L*), and accelerates RhoA degradation (Fig. 7*A–D*,*F*), partially explaining the redundancy between the kinases. Overexpression of activated Rac1 and depletion of RhoA acted synergistically to rescue neuronal migration in *Stk25*-deficient neurons (Fig. 9*A*,*B*). We found that STK25 acts via Cul3 and Bacurd1 to regulate both RhoA levels and Rac1 activity (Figs. 6*K*,*L*, 7*E–G*, 8*B–E*, 9*H*,*I*). STK25 also interacts with α-, β-PIXs providing another possible route to activate Rac1 (Fig. 6*J*). Taken together, these data suggest that STK25 regulates two different signaling pathways, STK25-Cul3-Bacurd1 to deplete RhoA and STK25-PIX to activate Rac1 in the regulation of corticogenesis.

STK25 and MST3 compensate for each other in neuronal migration and polarization

STK25 is known to play roles in axonogenesis, dendritogenesis, Golgi morphology, neuronal migration, and neuronal polarization (Matsuki et al., 2010, 2013; Huang et al., 2014; Mencarelli et al., 2018; Rao et al., 2018). Recently it has been shown that another GCKIII family member MST3 also regulates neuronal migration (Tang et al., 2014). We found that MST3 functionally compensates for *Stk25* deficiency and rescued proper migration and axon production during cortical development *in vivo*. We made use of the *Stk25*-conditional mice to get a sense of how long it takes for compensation to occur. MST3 levels were unaltered 2 d after *Stk25* gene inactivation (Fig. 5*A*,*B*), apparent in only a subset of neurons by 3 d (Fig. 5*H*,*J*) and ~30% higher by 4 d (Fig. 5*C*,*D*). Compensation is apparently not quick enough to support normal corticogenesis at 3 d after gene inactivation when examined at E17.5 (Fig. 1*D*). However, when we inactivated *Stk25* a week before analysis, neuronal migration appeared normal (Fig. 5*K*,*L*), suggesting that it takes between 3 and 7 d for restoration of sufficient GCKIII levels to compensate. This helps to explain the lack of cortical phenotype in the *Stk25-null* mutant and the neuronal-position defect observed after acute deletion of *Stk25* (Fig. 1*D*,*E*; Matsuki et al., 2013). MST3 levels also increased when STK25 expression was disrupted (Fig. 5*H*, *J*). The total amount of STK25 and/or MST3 in the same neuron may be important for proper neuronal migration through the Rac1 activation and RhoA destabilization (Figs. 5*I*,*J*, 6*K*,*L*, 8*B–E*). Similarly, STK25 overexpression rescued neuronal migration and polarization defects caused by *Mst3* knock-down *in vivo* (Fig. 1*F*,*G*). Four days after *Mst3* knock-down, the increase in STK25 expression appears to be more robust than the increase in MST3 expression in response to STK25 KO (350% vs 30%), suggesting that genetic compensation may be quicker in response to a deficit in *Mst3* (Fig. 5*F*,*G*).

While we previously showed that STK25 kinase activity was not required to rescue the neuronal positioning or polarization phenotypes, MST3's kinase activity is required for neuronal migration (Fig. 1*D*,*E*) but is not as important for neuronal polarization/axonogenesis (Figs. 2*A–C*, 3*B–G*). This is consistent with a previous report showing MST3's kinase activity was required to regulate neuronal positioning (Tang et al., 2014). This suggests that in addition to the phosphorylation of downstream targets these molecules have important roles as scaffolding molecules, which appears to be especially true for STK25, which appears to regulate Rac1 activity and RhoA levels through the formation of complexes with activators and ubiquitin ligases.

STK25 acts as a scaffolding protein to differentially regulate Rho GTPases

A previous study showed that MST3 interacts with RhoA and negatively regulates its activity by phosphorylation (Tang et al., 2014). The authors also showed that RhoA overexpression hinders proper neuronal migration. STK25 and MST3 are also capable of suppressing RhoA through the activation of Moesin (Zheng et al., 2010). Here, we found that in cells expressing the GCKIII kinases, RhoA levels were restored by drugs that inhibit either proteasomal or lysosomal degradation in STK25-, but only a lysosomal inhibitor in MST3-overexpressing cells (Fig. 7*C*,*D*). This suggests that MST3 amplifies lysosomal degradation while STK25 amplifies both lysosomal and proteasomal degradation. Combined with previous work, this suggests that RhoA is targeted by multiple downstream signaling events regulated by these kinases to reduce its activity or levels. Both STK25 and MST3 interact with the Cullins 1, 3, 4A, and 4B (Fig. 7*E*). In the case of Cul3, roles in both proteasomal and lysosomal

degradation have been shown (Huotari et al., 2012). STK25 also interacts with the Bacurd1 and Bacurd2 (Fig. 7*G*), which are also involved in RhoA degradation (Gladwyn-Ng et al., 2016). Unlike the case in *Mst3*-deficient neurons (Tang et al., 2014), however, knock-down of *RhoA* was not sufficient to rescue *Stk25*-deficient neurons, but it did act synergistically with overexpression of an activated mutant of Rac1 (Fig. 9*A*,*B*).

In addition to RhoA, we found that both STK25 and MST3 interact weakly with Cdc42 and robustly with Rac1 (Fig. 6*A*). STK25 also interacts with the Rac1 and Cdc42 GEFs, α-PIX and β-PIX (Fig. 6*J*). Not surprisingly therefore, we found that *Stk25* acute deletion transiently reduces Rac1-GTP levels in the E16.5 VZ/SVZ of the developing neocortex (Fig. 6*D*,*E*,*K*,*L*), but it was restored by E18.5 (Fig. 6*D*,*F*). Furthermore, reduced STK25 neuronal expression transiently reduces the association between Rac1 and the actin regulator and WAVE1 binding protein CYFIP1, in line with the reduced levels of Rac1-GTP (Fig. 6*G*,*H*). Activation appears to be critically important downstream of STK25, since it is capable of partially rescuing *Stk25* deficiency on its own and synergistically with augmented *RhoA* knock-down (Fig. 9*A*, *B*). Cul3 and Bucurd1, which are known for their role in RhoA degradation, were able to rescue neuronal migration in *Stk25*-deficient neurons whereas *RhoA* reduction alone did not (Fig. 9*A*–*F*). This presented a conundrum that led us to the discovery that these molecules, which act in concert, also elevate Rac1-GTP levels (Fig. 9*H*,*I*). Similarly, it has recently been shown that the Cul3/Bacurd3 complex is required for EGFR-induced Rac1 activation in cancer cells (Murakami et al., 2019). Thus, potentially two or more pathways exist downstream of STK25 that activate Rac1.

A previous study has shown roles for Rac1 and RhoA activity to regulate radial migration in neurons (Xu et al., 2015). In this regard, RhoA's active form is distributed on the side of contact between neurons and radial glial fibers. Since STK25 reduces RhoA levels this suggests that STK25 might act before the glial dependent migration phase. However, more detailed spatial and temporal resolution of the mechanism of STK25 regulated neuronal migration are warranted. It remains to be determined whether Rac1 is also activated downstream of MST3, but based on MST3 interactions with Rac1, and α-PIX and β-PIX this seems likely.

In sum, in this study, we have elucidated that STK25 and MST3 compensate for each other to regulate neuronal migration and cell and neuronal polarization. We found that STK25 has a role to upregulate Rac1 activity and downregulate RhoA stability. Active Rac1 is required for forward migration, whereas increased RhoA expression suppresses migration. Thus, STK25 appears to fine tune the activity and levels of these Rho GTPases to coordinate neuronal migration. Mechanistically STK25 interacts with Cul3-Bacurd1 to regulate both RhoA levels and Rac1 activity highlighting a key role for these molecules in the regulation of cortical lamination. Our study has uncovered new mechanistic consequences of STK25 signaling, providing new insights into the genetic compensatory processes at play during mammalian brain development.

References

Amrutkar M, Chursa U, Kern M, Nuñez-Durán E, Ståhlman M, Sütt S, Borén J, Johansson BR, Marschall HU, Blüher M, Mahlapuu M (2016) STK25 is a critical determinant in nonalcoholic steatohepatitis. FASEB J 30:3628–3643.

Anitei M, Stange C, Parshina I, Baust T, Schenck A, Raposo G, Kirchhausen T, Hoflack B (2010) Protein complexes containing CYFIP/Sra/PIR121 coordinate Arf1 and Rac1 signalling during clathrin-AP-1-coated carrier biogenesis at the TGN. Nat Cell Biol 12:330–340.

Baas AF, Kuipers J, van der Wel NN, Batlle E, Koerten HK, Peters PJ, Clevers HC (2004) Complete polarization of single intestinal epithelial cells upon activation of LKB1 by STRAD. Cell 116:457–466.

Bae SJ, Ni L, Luo X (2020) STK25 suppresses Hippo signaling by regulating SAV1-STRIPAK antagonism. Elife 9:e54863.

Baird D, Feng Q, Cerione RA (2005) The Cool-2/alpha-Pix protein mediates a Cdc42-Rac signaling cascade. Curr Biol 15:1–10.

Barnes AP, Polleux F (2009) Establishment of axon-dendrite polarity in developing neurons. Annu Rev Neurosci 32:347–381.

Barnes AP, Lilley BN, Pan YA, Plummer LJ, Powell AW, Raines AN, Sanes JR, Polleux F (2007) LKB1 and SAD kinases define a pathway required for the polarization of cortical neurons. Cell 129:549–563.

Chen L, Liao G, Waclaw RR, Burns KA, Linquist D, Campbell K, Zheng Y, Kuan CY (2007) Rac1 controls the formation of midline commissures and the competency of tangential migration in ventral telencephalic neurons. J Neurosci 27:3884–3893.

Chen Y, Yang Z, Meng M, Zhao Y, Dong N, Yan H, Liu L, Ding M, Peng HB, Shao F (2009) Cullin mediates degradation of RhoA through evolutionarily conserved BTB adaptors to control actin cytoskeleton structure and cell movement. Mol Cell 35:841–855.

Cooper JA (2014) Molecules and mechanisms that regulate multipolar migration in the intermediate zone. Front Cell Neurosci 8:386.

El-Brolosy MA, Stainier DYR (2017) Genetic compensation: a phenomenon in search of mechanisms. PLoS Genet 13:e1006780.

Escamilla CO, Filonova I, Walker AK, Xuan ZX, Holehonnur R, Espinosa F, Liu S, Thyme SB, López-García IA, Mendoza DB, Usui N, Ellegood J, Eisch AJ, Konopka G, Lerch JP, Schier AF, Speed HE, Powell CM (2017) Kctd13 deletion reduces synaptic transmission via increased RhoA. Nature 551:227–231.

Fan L, Lu Y, Shen X, Shao H, Suo L, Wu Q (2018) Alpha protocadherins and Pyk2 kinase regulate cortical neuron migration and cytoskeletal dynamics via Rac1 GTPase and WAVE complex in mice. Elife 7:e35242.

Gladwyn-Ng I, Huang L, Ngo L, Li SS, Qu Z, Vanyai HK, Cullen HD, Davis JM, Heng JI (2016) Bacurd1/Kctd13 and Bacurd2/Tnfaip1 are interacting partners to Rnd proteins which influence the long-term positioning and dendritic maturation of cerebral cortical neurons. Neural Dev 11:7.

Govek EE, Hatten ME, Van Aelst L (2011) The role of Rho GTPase proteins in CNS neuronal migration. Dev Neurobiol 71:528–553.

Higashi M, Yu J, Tsuchiya H, Saito T, Oyama T, Kawana H, Kitagawa M, Tamaru J, Harigaya K (2010) Visualization of the activity of Rac1 small GTPase in a cell. Acta Histochem Cytochem 43:163–168.

Huang W, She L, Chang XY, Yang RR, Wang L, Ji HB, Jiao JW, Poo MM (2014) Protein kinase LKB1 regulates polarized dendrite formation of adult hippocampal newborn neurons. Proc Natl Acad Sci USA 111:469–474.

Huotari J, Meyer-Schaller N, Hubner M, Stauffer S, Katheder N, Horvath P, Mancini R, Helenius A, Peter M (2012) Cullin-3 regulates late endosome maturation. Proc Natl Acad Sci USA 109:823–828.

Itoh RE, Kurokawa K, Ohba Y, Yoshizaki H, Mochizuki N, Matsuda M (2002) Activation of rac and cdc42 video imaged by fluorescent resonance energy transfer-based single-molecule probes in the membrane of living cells. Mol Cell Biol 22:6582–6591.

Kawauchi T (2011) Regulation of cell adhesion and migration in cortical neurons: not only Rho but also Rab family small GTPases. Small GTPases 2:36–40.

Kawauchi T (2015) Cellullar insights into cerebral cortical development: focusing on the locomotion mode of neuronal migration. Front Cell Neurosci 9:394.

Kholmanskikh SS, Dobrin JS, Wynshaw-Boris A, Letourneau PC, Ross ME (2003) Disregulated RhoGTPases and actin cytoskeleton contribute to the migration defect in Lis1-deficient neurons. J Neurosci 23:8673–8681.

Kholmanskikh SS, Koeller HB, Wynshaw-Boris A, Gomez T, Letourneau PC, Ross ME (2006) Calcium-dependent interaction of Lis1 with IQGAP1 and Cdc42 promotes neuronal motility. Nat Neurosci 9:50–57.

Kurokawa K, Itoh RE, Yoshizaki H, Nakamura YO, Matsuda M (2004) Coactivation of Rac1 and Cdc42 at lamellipodia and membrane ruffles induced by epidermal growth factor. Mol Biol Cell 15:1003–1010.

Lawson CD, Ridley AJ (2018) Rho GTPase signaling complexes in cell migration and invasion. J Cell Biol 217:447–457.

Lim S, Hermance N, Mudianto T, Mustaly HM, Mauricio IPM, Vittoria MA, Quinton RJ, Howell BW, Cornils H, Manning AL, Ganem NJ (2019) Identification of the kinase STK25 as an upstream activator of LATS signaling. Nat Commun 10:1547.

Lin GN, Corominas R, Lemmens I, Yang X, Tavernier J, Hill DE, Vidal M, Sebat J, Iakoucheva LM (2015) Spatiotemporal 16p11.2 protein network implicates cortical late mid-fetal brain development and KCTD13-Cul3-RhoA pathway in psychiatric diseases. Neuron 85:742–754.

Lorber B, Howe ML, Benowitz LI, Irwin N (2009) Mst3b, an Ste20-like kinase, regulates axon regeneration in mature CNS and PNS pathways. Nat Neurosci 12:1407–1414.

Matsuda T, Cepko CL (2007) Controlled expression of transgenes introduced by in vivo electroporation. Proc Natl Acad Sci USA 104:1027–1032.

Matsuki T, Chen J, Howell BW (2013) Acute inactivation of the serine-threonine kinase Stk25 disrupts neuronal migration. Neural Dev 8:21.

Matsuki T, Matthews RT, Cooper JA, van der Brug MP, Cookson MR, Hardy JA, Olson EC, Howell BW (2010) Reelin and stk25 have opposing roles in neuronal polarization and dendritic Golgi deployment. Cell 143:826–836.

Mencarelli C, Nitarska J, Kroecher T, Ferraro F, Massey K, Riccio A, Pichaud F (2018) RanBP1 couples nuclear export and Golgi regulation through LKB1 to promote cortical neuron polarity. Cell Rep 24:2529–2539.e4.

Murakami A, Maekawa M, Kawai K, Nakayama J, Araki N, Semba K, Taguchi T, Kamei Y, Takada Y, Higashiyama S (2019) Cullin-3/KCTD10 E3 complex is essential for Rac1 activation through RhoB degradation in human epidermal growth factor receptor 2-positive breast cancer cells. Cancer Sci 110:650–661.

Nethe M, Hordijk PL (2010) The role of ubiquitylation and degradation in RhoGTPase signalling. J Cell Sci 123:4011–4018.

Niwa H, Yamamura K, Miyazaki J (1991) Efficient selection for high-expression transfectants with a novel eukaryotic vector. Gene 108:193–199.

Olenik C, Aktories K, Meyer DK (1999) Differential expression of the small GTP-binding proteins RhoA, RhoB, Cdc42u and Cdc42b in developing rat neocortex. Brain Res Mol Brain Res 70:9–17.

Pacary E, Heng J, Azzarelli R, Riou P, Castro D, Lebel-Potter M, Parras C, Bell DM, Ridley AJ, Parsons M, Guillemot F (2011) Proneural transcription factors regulate different steps of cortical neuron migration through Rnd-mediated inhibition of RhoA signaling. Neuron 69:1069–1084.

Preisinger C, Short B, De Corte V, Bruyneel E, Haas A, Kopajtich R, Gettemans J, Barr FA (2004) YSK1 is activated by the Golgi matrix protein GM130 and plays a role in cell migration through its substrate 14-3-3zeta. J Cell Biol 164:1009–1020.

Rao S, Kirschen GW, Szczurkowska J, Di Antonio A, Wang J, Ge S, Shelly M (2018) Repositioning of somatic Golgi apparatus is essential for the dendritic establishment of adult-born hippocampal neurons. J Neurosci 38:631–647.

Sailland J, Tribollet V, Forcet C, Billon C, Barenton B, Carnesecchi J, Bachmann A, Gauthier KC, Yu S, Giguère V, Chan FL, Vanacker JM (2014) Estrogen-related receptor α decreases RHOA stability to induce orientated cell migration. Proc Natl Acad Sci USA 111:15108–15113.

Schaks M, Singh SP, Kage F, Thomason P, Klünemann T, Steffen A, Blankenfeldt W, Stradal TE, Insall RH, Rottner K (2018) Distinct interaction sites of Rac GTPase with WAVE regulatory complex have non-redundant functions in vivo. Curr Biol 28:3674–3684.e6.

Shelly M, Cancedda L, Heilshorn S, Sumbre G, Poo MM (2007) LKB1/STRAD promotes axon initiation during neuronal polarization. Cell 129:565–577.

Simó S, Cooper JA (2013) Rbx2 regulates neuronal migration through different cullin 5-RING ligase adaptors. Dev Cell 27:399–411.

Steffen A, Rottner K, Ehinger J, Innocenti M, Scita G, Wehland J, Stradal TE (2004) Sra-1 and Nap1 link Rac to actin assembly driving lamellipodia formation. EMBO J 23:749–759.

Tahirovic S, Hellal F, Neukirchen D, Hindges R, Garvalov BK, Flynn KC, Stradal TE, Chrostek-Grashoff A, Brakebusch C, Bradke F (2010) Rac1 regulates neuronal polarization through the WAVE complex. J Neurosci 30:6930–6943.

Tang J, Ip JP, Ye T, Ng YP, Yung WH, Wu Z, Fang W, Fu AK, Ip NY (2014) Cdk5-dependent Mst3 phosphorylation and activity regulate neuronal migration through RhoA inhibition. J Neurosci 34:7425–7436.

ten Klooster JP, Jaffer ZM, Chernoff J, Hordijk PL (2006) Targeting and activation of Rac1 are mediated by the exchange factor beta-Pix. J Cell Biol 172:759–769.

Xu C, Funahashi Y, Watanabe T, Takano T, Nakamuta S, Namba T, Kaibuchi K (2015) Radial glial cell-neuron interaction directs axon formation at the opposite side of the neuron from the contact site. J Neurosci 35:14517–14532.

Zheng X, Xu C, Di Lorenzo A, Kleaveland B, Zou Z, Seiler C, Chen M, Cheng L, Xiao J, He J, Pack MA, Sessa WC, Kahn ML (2010) CCM3 signaling through sterile 20-like kinases plays an essential role during zebrafish cardiovascular development and cerebral cavernous malformations. J Clin Invest 120:2795–2804.